Energy Conversion and Management 148 (2017) 1508–1524

Contents lists available at ScienceDirect

Energy Conversion and Management

journal homepage: www.elsevier.com/locate/enconman

Performance of working-fluid mixtures in ORC-CHP systems for different heat-demand segments and heat-recovery temperature levels

Oyeniyi A. Oyewunmi [a], Christoph J.W. Kirmse [a], Antonio M. Pantaleo [a,b], Christos N. Markides [a,*]

[a] Clean Energy Processes (CEP) Laboratory, Department of Chemical Engineering, Imperial College London, South Kensington Campus, London SW7 2AZ, United Kingdom
[b] Department of Agro-Environmental and Landscape Sciences, University of Bari, Via Orabona 3, 70125 Bari, Italy

ARTICLE INFO

Article history:
Received 8 February 2017
Received in revised form 30 May 2017
Accepted 31 May 2017

Keywords:
Organic Rankine cycle (ORC)
Combined heat and power (CHP)
Heat recovery
Working-fluid mixtures
Thermal energy demand

ABSTRACT

In this paper, we investigate the adoption of working-fluid mixtures in ORC systems operating in combined heat and power (CHP) mode, with a power output provided by the expanding working fluid in the ORC turbine and a thermal energy output provided by the cooling water exiting (as a hot-water supply) the ORC condenser. We present a methodology for selecting optimal working-fluids in ORC systems with optimal CHP heat-to-electricity ratio and heat-supply temperature settings to match the seasonal variation in heat demand (temperature and intermittency of the load) of different end-users. A number of representative industrial waste-heat sources are considered by varying the ORC heat-source temperature over the range 150–330 °C. It is found that, a higher hot-water outlet temperature increases the exergy of the heat-sink stream but decreases the power output of the expander. Conversely, a low outlet temperature (~30 °C) allows for a high power-output, but a low cooling-stream exergy and hence a low potential to heat buildings or to cover other industrial thermal-energy demands. The results demonstrate that the optimal ORC shaft-power outputs vary considerably, from 9 MW up to 26 MW, while up to 10 MW of heating exergy is provided, with fuel savings in excess of 10%. It also emerges that single-component working fluids such as *n*-pentane appear to be optimal for fulfilling low-temperature heat demands, while working-fluid mixtures become optimal at higher heat-demand temperatures. In particular, the working-fluid mixture of 70% *n*-octane + 30% *n*-pentane results in an ORC-CHP system with the highest ORC exergy efficiency of 63% when utilizing 330 °C waste heat and delivering 90 °C hot water. The results of this research indicate that, when optimizing the global performance of ORC-CHP systems fed by industrial waste-heat sources, the temperature and load pattern of the cogenerated heat demand are crucial factors affecting the selection of the working fluid.

1. Introduction

The rising global demand for energy and increasing desire for sustainable, secure energy provision are major drivers for enhancing the efficiency of energy processes and systems. The particular, the utilization of the considerable quantities of wasted heat that are available in large quantities from numerous sources in the industrial, tertiary, residential and transportation sectors is a promising way of achieving an increase in overall system efficiency [1]. At the same time, renewable sources of low- and medium-grade (temperature) heat, such as solar or geothermal heat, can play a key role in displacing the consumption of primary energy (fossil fuels) [2]. Low- and medium-grade waste or renewable heat can be converted into useful power such as electricity, or recovered to provide heating directly to buildings (for hot water or space heating), or a combination of the two. A number of technologies exist for the conversion of lower-grade heat to power. The Kalina cycle, for example, uses a mixture of ammonia and water, whereas organic Rankine cycles (ORCs) can employ different organic working fluids such as hydrocarbons, refrigerants or siloxanes [3–6], or mixtures thereof. A significant effort has been placed on the development and improvement of ORC power systems in different applications [7–13], usually at plant scales in the ~1–10 MW range.

The thermal efficiency attainable by thermodynamic power-cycles is inherently low in the case of lower-grade heat-conversion technologies compared to conventional (*e.g.*, fossil fuel or nuclear) power plants. In those applications, however, the thermal efficiency is not the only, nor the most important performance indicator, with economic factors (*e.g.*, payback, specific cost, NPV) playing a dominant role in determining whether relevant projects and solutions are economically viable and of financing interest to investors.

* Corresponding author.
E-mail address: c.markides@imperial.ac.uk (C.N. Markides).

http://dx.doi.org/10.1016/j.enconman.2017.05.078
0196-8904/

Nomenclature

c_p	specific heat capacity at constant pressure, J/(kg K)
$\dot{E}$	exergy flow-rate, W
h	specific enthalpy, J/kg
h	yearly operating hours, hours/year
$\dot{m}$	mass flow rate, kg/s
P	pressure, Pa or bar
$\dot{Q}$	heat flow-rate, W
s	specific entropy, J/(kg K)
T	temperature, °C or K
$\dot{W}$	power, W
x	mass fraction
x_{CHP}	ratio of operating hours to available hours

Greek symbols

η	efficiency, %
θ_{sh}	degree of superheating

Subscripts and superscripts

0	reference state
1	ORC condenser outlet/pump inlet
2	ORC pump outlet/evaporator inlet
3	ORC evaporator outlet/expander inlet
4	ORC expander outlet/condenser inlet
CHP	combined heat and power system
cond	condensation
crit	critical
cs	cooling sink (building heating supply)
dew	dew point
evap	evaporation
ex	exergy
exp	expander
hs	heat source
in	inlet
min	minimum
ORC	organic Rankine cycle
out	outlet
pump	pump
s	isentropic
SH	space heating
su	hot-water supply temperature
th	thermal
TOT	total
wf	working fluid

Nevertheless, at least from a purely thermodynamic perspective, the overall efficiency of industrial or urban energy systems can be directly enhanced by recovering and utilizing wasted heat. Once the heat-recovery infrastructure is in place and no significant further costs are incurred in continuously generating the energy input (waste heat in this case), the baseload waste-heat recovery operation that maximizes the power output is often the most profitable strategy. Additional benefits may be realized by serving low-temperature heat demands with the discharged cogenerated heat as in other waste-heat or renewable (*e.g.*, solar) combined heat and power (CHP) applications, thus significantly increasing the global or overall efficiency of the system (*i.e.*, ratio of useful total energy delivered in the form of both heat and electricity to the heat input) [14–20].

Although an increase in the heat-sink temperature increases the usefulness of the thermal output delivered to the demand, it may also act to reduce the power output. Earlier work in Ref. [3] considered large temperature-glide organic-fluid mixtures in the context of cogeneration from ORC systems (or, limited coolant resources), while focussing on the power output only. The mixtures were found to be optimal in terms of power output, due to an improved thermal match of the cycle to the waste-heat source and the heat-demand profile, suggesting that considerations based on balancing the thermal and electrical outputs may not always be unavoidably in conflict, and motivating the work this present paper whose aim is to explore mixtures in CHP-ORC systems.

A number of research efforts have focused on the optimal selection of the heat-to-electricity ratio in ORC-CHP systems in order to maximize the global energy system performance on the basis of different heat-demand profiles, the quality of thermal energy required by the load and the influence of the discharged heat sink on the CHP output power [21,22]. Other studies have focused on the part-load efficiency of different CHP configurations and selection of the best operational strategies on the basis of the electricity and heat-demand profiles [23,24]. In this paper, we consider waste-heat recovery from flue-gas streams over a range of temperatures from 150 °C to 330 °C and mass flow-rates from 120 kg/s and 560 kg/s for utilization in an ORC-CHP configuration. Thus, shaft power is generated by thermodynamic conversion in the ORC turbine, while a thermal output is provided for space heating provision to blocks of residential/tertiary buildings or (more steady) industrial heat demands by the cooling stream in the ORC condenser. Beyond evaluating conventional CHP metrics, the quality of the heating stream is quantified by evaluating its increase in exergy flow-rate through the ORC condenser, based on which two exergy efficiency measures for the ORC-CHP system are calculated as the sum of the ORC power output and the exergy flow-rate of the heat generation. These efficiency measures are optimized for different outlet temperatures of the ORC condenser stream, with *n*-alkane and refrigerant working-fluids, and their binary mixtures.

It is noted that, in general, the waste-heat supply and the low-temperature heat-demand profiles will not be matched. In particular, industrial waste-heat is strictly related to specific industrial processes and that even when this is relatively steady the heat-demand profiles of buildings are strongly affected by daily and seasonal variations. This means that, without suitable thermal storage systems, cogenerated heat from ORC-CHP systems can be discharged over large periods of the year, and is especially true when waste-heat availability makes it profitable in baseload CHP operation to maximize power output, instead of thermal load following operations. The best working fluid for a given heat-demand temperature resulting from the optimization procedure may not be the optimal one if the heat demand is affected by high temporal variations and does not match the CHP output profile. This is of particular interest in the present work. For this reason, the influence of heat-demand profile on optimal working-fluid selection and CHP conversion efficiency is also explored.

2. Working-fluid selection for ORC systems

An extensive review of working fluids and their selection for ORC applications according to thermodynamic performance indicators and environmental or safety aspects is given in Bao and Zhao [25]. In the current paper, we do not intend to give an expansive review of working fluids for ORC applications. However, we will briefly discuss the advantages and disadvantages of the considered pure working fluids and working-fluid mixtures that are used in

this work. The pure working fluids are the *n*-alkanes from *n*-butane to *n*-octane, and the refrigerants R245fa and R227ea. Those fluids are dry fluids with the exception of R245fa, which is an isentropic fluid [26,27]. The advantage of dry and isentropic working fluids is that they are in the vapor phase after expansion, unlike wet fluids (*e.g.*, water) that can after expansion be in the two-phase region.

One advantage of the *n*-alkanes over the aforementioned two refrigerants is their low global warming potential (GWP) [27]. For example, *n*-butane and *n*-pentane have GWPs of 4, while R245fa has a GWP of 1030 and R227ea has a GWP of 3200. However, the flammability of *n*-alkanes limits their applicability, especially for high temperature applications, whereas R227ea and R245fa are non-flammable. One way to overcome this restriction is to mix the hydrocarbons with non-flammable refrigerants, which can act as a retardant [28,29].

The refrigerants R227ea and R245fa have been investigated in many studies [26,30,31]. For geothermal sources, it was found that R245fa has a higher net power output and thermal efficiency than *n*-butane or *n*-pentane [31], while R227ea was found to have the highest net power output amongst a pool of about 200 working fluids [30]. Furthermore, experimental investigations have been undertaken with those refrigerants and different expander types (*e.g.*, radial turbine and screw expander) [32–34]. The five *n*-alkanes considered in this work have been widely used in the literature for heat source temperatures between 100 °C and 520 °C [9,27,35,36]. The applications include geothermal heat-sources and waste-heat recovery, *e.g.*, from Diesel-cycle engines.

3. Methodology

3.1. Thermodynamic ORC model

The ORC-CHP systems considered in this work, consist of an ORC unit for power generation and a CHP section for space heating in residential and industrial buildings. In the ORC unit, heat is recovered from waste flue gas (and transferred to the working fluid) in the evaporator, while power is generated by the expansion of the working fluid through a suitable expander. Heat rejected from the working fluid to the cooling stream in the condenser serves as the heat source for the CHP unit. While condensing the working fluid, the temperature of the cooling stream is raised and it becomes warm. The 'warm' cooling stream is then fed to heating systems in the buildings, providing heat and thereby attaining a lower temperature. This low-temperature stream is then fed back to the condenser to extract heat from the working fluid and the cycle is repeated continuously.

A schematic diagram of the ORC-CHP system architecture along with corresponding temperature – specific entropy (*T*–*s*) diagrams for non-recuperative cycles are presented in Fig. 1. The working-fluid states in the system schematic correspond to those in the cycle diagram, and *vice versa*.

The required power of the pump is modelled by using the following equation:

$$\dot{W}_{\text{pump}} = \dot{m}_{\text{wf}}(h_2 - h_1) = \frac{\dot{m}_{\text{wf}}(h_{2,s} - h_1)}{\eta_{\text{s,pump}}}, \tag{1}$$

where $\dot{m}_{\text{wf}}$ is the mass flow rate of the working fluid, h is the enthalpy and $\eta_{\text{s,pump}}$ is the isentropic efficiency of the pump, which is set to 75%.

In the evaporator, the minimum pinch temperature-difference ΔT_{min} is set to 10 °C. It is assumed that there are no heat losses in the heat exchanger. The temperature of the working fluid at State 3 can vary between the dew point temperature at the evaporation pressure (no superheating) and its maximum temperature (when the pinch point is at the heat source inlet, *i.e.*, $T_{\text{hs}} - \Delta T_{\text{min}}$), corresponding to the maximum degree of superheating (θ_{sh}):

$$\theta_{\text{sh}} = \frac{T_3 - T_{\text{dew}}(P_{\text{evap}})}{T_{\text{hs}} - \Delta T_{\text{min}} - T_{\text{dew}}(P_{\text{evap}})}. \tag{2}$$

Assuming an isobaric heat-addition process, the rate of heat input from the heat source is given by:

$$\dot{Q}_{\text{in}} = \dot{m}_{\text{wf}}(h_3 - h_2) = \dot{m}_{\text{hs}} c_{\text{p,hs}}(T_{\text{hs,in}} - T_{\text{hs,out}}), \tag{3}$$

where $c_{\text{p,hs}}$ is the specific heat capacity of the heat-source stream.

The exergy flow-rate drop in the heat-source stream associated with the above heat input is:

$$\dot{E}_{\text{in}} = \dot{m}_{\text{hs}}[c_{\text{p,hs}}(T_{\text{hs,in}} - T_{\text{hs,out}}) - T_0(s_{\text{hs,in}} - s_{\text{hs,out}})], \tag{4}$$

where s is the specific entropy and T_0 the reference 'dead-state' temperature, which is set to ambient temperature in this work (20 °C).

The power that can be extracted from the cycle in the expander is given by:

$$\dot{W}_{\text{exp}} = \dot{m}_{\text{wf}}(h_3 - h_4) = \eta_{\text{s,exp}}\dot{m}_{\text{wf}}(h_3 - h_{4,s}), \tag{5}$$

with the isentropic efficiency of the expander $\eta_{\text{s,exp}}$ set to 75%, which is in the lower range of literature values, and hence a conservative measure [37–40].

Heat from the cycle is rejected in the condenser to the heat sink. The heat sink stream is utilized to provide heating to cover a low-temperature heat demand. The heat rejected from the cycle is:

$$\dot{Q}_{\text{out}} = \dot{Q}_{\text{SH}} = \dot{m}_{\text{wf}}(h_4 - h_1) = \dot{m}_{\text{cs}} c_{p,\text{cs}}(T_{\text{cs,out}} - T_{\text{cs,in}}). \tag{6}$$

Similar to the evaporator, the pinch temperature-difference in the condenser is set to 10 °C. The inlet temperature of the heat sink $T_{\text{cs,in}}$ is set to 20 °C, while the outlet temperature $T_{\text{cs,out}}$ can vary between 30 °C and 90 °C. This temperature is equal to the supply temperature of the heat stream that is used to serve the heat demand. The return temperature of this stream is set to 30 °C, so that for $T_{\text{cs,out}}$ = 30 °C no heating is provided and for $T_{\text{cs,out}}$ = 90 °C the maximum heating is provided.

To quantify the quality of the heat rejected to the cooling stream/sink from the ORC engine, the rise in the exergy flow-rate of this heat-supply stream through the CHP system is calculated from:

$$\dot{E}_{\text{SH}} = \dot{m}_{\text{cs}}[c_{\text{p,cs}}(T_{\text{cs,out}} - T_{\text{cs,in}}) - T_0(s_{\text{cs,out}} - s_{\text{cs,in}})], \tag{7}$$

which is taken to be a measure of the exergy in the stream available for heating.

Along with the net power output and the heating exergy, the third performance indicator for the ORC engine considered in this paper is the ORC exergy efficiency, which combines the power output from the ORC engine and the exergy flow-rate in the heat-supply stream [41–46]:

$$\eta_{\text{ex,ORC}} = \frac{(\dot{W}_{\text{exp}} - \dot{W}_{\text{pump}}) + \dot{E}_{\text{SH}}}{\dot{E}_{\text{in}}}. \tag{8}$$

The above-mentioned performance indicators go beyond the traditional 'energy utilization factor' EUF (also referred to as a total or overall efficiency) and 'fuel-energy savings ratio' FESR of CHP systems, nevertheless, salient EUF and FESR values are also mentioned in this paper for the purposes of comparison and benchmarking. The FESR is defined as the fuel saved in a CHP plant relative to the fuel needed to meet the separate electrical and heat demands by separate dedicated conventional plants; the electrical efficiency and boiler efficiency values for the conventional plants are taken here to be 40% and 85% respectively. In this paper, the initial heat source considered is a flue gas from an industrial process with a mass flow rate

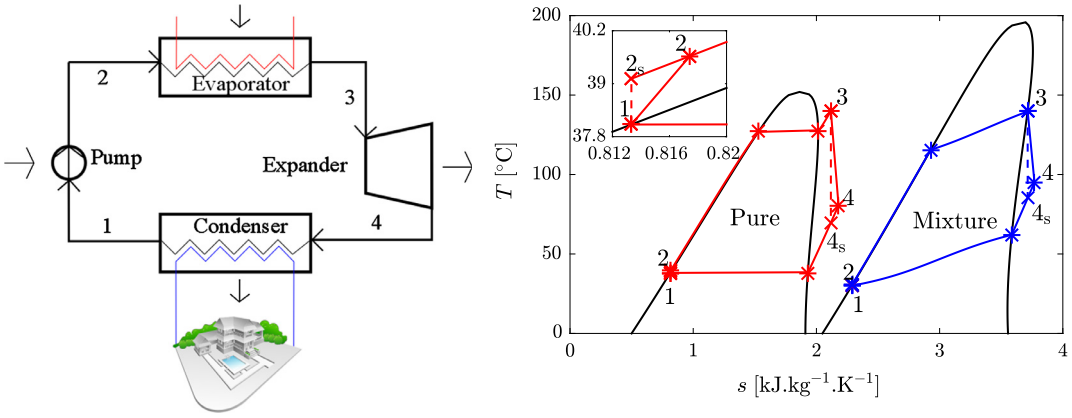

Fig. 1. Schematic of the non-recuperative ORC-CHP system component architecture, and T–s diagram of the cycle for a dry single-component (pure) working fluid with superheating and a multi-component (mixture) working fluid without superheating, showing the temperature glides during the evaporation and condensation of the working fluid.

of 560 kg/s and the temperature at the inlet of 330 °C. This represents a typical high-temperature industrial waste-heat source; later on, medium-temperature (250 °C) and low-temperature (150 °C) heat sources are considered with mass flow-rates of 120 kg/s and 30 kg/s, respectively, illustrated with the results presented in Sections 4.3 and 4.4.

3.2. Optimization algorithm

An optimization algorithm is employed to find the maximum exergy efficiency of the aforementioned CHP system, which necessitates an objective function and constraints to be defined:

$$\max\{\eta_{ex}\} \tag{9}$$

$$\text{s.t.}\Delta T_{min} \geqslant 10^{\circ}\text{C} \tag{10}$$

$$T_4 \geqslant T_{dew}(P_{cond}) \tag{11}$$

$$P_{evap} \leqslant P_{crit} \tag{12}$$

$$0 \leqslant \theta_{sh} \leqslant 1 \tag{13}$$

$$P_{cond} \geqslant 1 \text{ bar} \tag{14}$$

The first constraint (Eq. (10)) ensures that the pinch conditions in the evaporator and condenser are satisfied. The temperature at the turbine T_4 outlet has to be higher than or equal to the dew point temperature at the condensation pressure (Eq. (11)) to prevent liquid droplet formation in the expander. This means that working fluid at the turbine outlet is always in the vapor state. For the cycle to be subcritical, the evaporation pressure has to be lower than or equal to the critical pressure (Eq. (12)). In addition, by definition, the degree of superheating must be between 0 and 1 (Eq. (13)). Finally (Eq. (14)), the condensation pressure must be equal to or larger than 1 bar (ambient) to avoid sub-atmospheric pressures in the cycle and expensive solutions to avoid air ingress.

3.3. ORC working-fluid selection

In this paper, we consider both pure working-fluids and working-fluid mixtures. The pure working-fluids are the refrigerants R245fa and R227ea, and the *n*-alkanes from *n*-butane to *n*-octane. We also consider binary mixtures of promising pure fluids. While single-component working-fluids evaporate isothermally at isobaric conditions, fluid mixtures exhibit a non-isothermal evaporation ('glide') as shown in Fig. 1, which can, in some cases, be used to raise the average temperature of heat addition. This is advantageous for the efficiency of an ORC-CHP system, since the temperature profile of the heat source can be matched by the working fluid, reducing losses in the evaporator. Similarly, the heat rejection process is non-isothermal for mixtures, which may raise the average temperature of heat rejection. This is expected to be detrimental for the cycle efficiency [47,48]. However, given that the heat sink is used to provide useful heating, the temperature profile of the heat sink can be better matched by using a working-fluid mixture, which can improve the overall exergy performance of the system. In recent years, working-fluid mixtures have attracted great attention in the literature, especially mixtures of the aforementioned pure fluids [7,10,13,49–51]. It should be noted that the working-fluid mixtures considered in this work are assumed to form perfect physically miscible pairs, and also not to be chemically reactive.

3.4. Energy-demand modelling and global CHP exergy efficiency

In order to account for the influence of the heat-demand profile on the global energy conversion efficiency of the CHP system, the coefficient x_{CHP} is introduced, which represents the ratio of equivalent operating hours h_{CHP} of the system in cogenerative operation (when both heating and power are delivered) to the total operating hours h_{TOT} over a yearly time horizon:

$$x_{CHP} = \frac{h_{CHP}}{h_{TOT}}. \tag{15}$$

This coefficient represents the fraction of generated thermal energy at the CHP plant that is delivered to the energy demand/sink as useful heat, and is a means of taking into account the temporal variations in the end-user's heat demand profile over a given time interval (typically, one year). In the case of baseload CHP operation (h_{TOT} of 7500 h/year), this coefficient typically ranges between 0.15 and 0.25 for residential heat demands, 0.2–0.3 for tertiary heat demands, and 0.40–0.65 for energy-intensive industrial demands; it is affected, case by case, by factors such as climatic conditions, building energy efficiency, industrial process operations, *etc.* [52–54].

The global exergy efficiency of the CHP system $\eta_{ex,CHP}$ over a year can be calculated from:

$$\eta_{ex,CHP} = \frac{(\dot{W}_{exp} - \dot{W}_{pump}) + \dot{E}_{SH} x_{CHP}}{\dot{E}_{in}}. \tag{16}$$

The CHP exergy efficiency ($\eta_{ex,CHP}$) differs from the ORC exergy efficiency ($\eta_{ex,ORC}$) defined in Eq. (8), in that it considers the utilization

of the generated heat by the end-user. The two definitions become equivalent when the available heat is fully utilized all year round, *i.e.*, if/when $x_{CHP} = 1$.

4. Results and discussion

In this section, results are presented concerning the following indices of comparison: net power output (Eq. (5)), heating capacity (Eq. (6)), heat-demand exergy (Eq. (7)), ORC and CHP-exergy efficiencies (Eqs. (8) and (16)), EUF and FESR. The heat-demand exergy is the exergy rise of the cooling water stream through the ORC condenser that can then be used to provide low-temperature heating to surrounding buildings or other demand segments. Results relating to working-fluid selection and subsequent ORC-CHP system performance are presented in Sections 4.1 and 4.2 for the aforementioned high-temperature heat source (330 °C, 560 kg/s) and in Section 4.3 we investigate the impact of the heat-source temperature (250 °C, 120 kg/s and 150 °C, 30 kg/s).

4.1. Performance of pure working-fluids

In this first instance, the ORC-CHP model was optimized with different working fluids while considering heat recovery and conversion from the high-temperature heat source ($T_{hs} = 330$ °C, $\dot{m}_{hs} = 560$ kg/s), by maximizing the ORC exergy efficiency at different hot-water supply temperatures and assuming $x_{CHP} = 1$. In Fig. 2, the maximum exergy-efficiency and the corresponding net power-output and heat-demand exergy of the system are presented as functions of the hot-water supply temperature, which is varied from 30 °C to 90 °C. The optimal design variables are also presented in Table 1 for the cases of hot-water supply at temperatures of 30 °C and 90 °C.

For all the working fluids considered here, the net power-output generally decreases with the hot-water supply temperature (this is also the temperature of the cooling water exiting the ORC engine). The ORC inlet cooling water is provided at 20 °C, thus higher exit temperatures imply larger temperature gradients across the condenser. This has the tendency of increasing the working fluid condensation temperature and pressure thereby reducing the power output from the ORC expander. Evidence of this is found in Table 1 where the condensation pressures of *n*-pentane and R245fa are more than doubled when the supply temperature is increased from 30 °C to 90 °C.

The effects of the operating conditions on the optimal exergy-efficiency of the ORC-CHP system are summarized in Table 1. Due to the high temperature of the heat source (which is higher than the critical temperatures of the working fluids) and the sub-critical nature of the ORC-CHP architecture, which is imposed by design, the optimal evaporation pressure is limited by the critical pressure such that it remains unaffected by the hot-water supply temperature. This is seen in Table 1, where the optimal evaporation pressures for the 30 °C and 90 °C cases are equal for each of the working fluids. The optimal condensation pressure, however, varies with the heat-supply temperature as noted earlier, and only with some fluids (*n*-heptane and *n*-octane) is it limited by the atmospheric pressure. The optimal mass flow-rate is that which maintains the pinch temperature-difference in the evaporator at the minimum specified value of 10 °C (Eq. (10)). The optimal superheating degree increases with the heat-supply temperature except for very dry fluids, specifically *n*-heptane and *n*-octane, for which it is negligible. This is a specific feature of these fluids, where optimal performance is attained by direct expansion from the saturated vapor line, without superheating.

For working fluids such as *n*-hexane, *n*-heptane and *n*-octane, the ORC net power output is seen (from Fig. 2) to remain constant

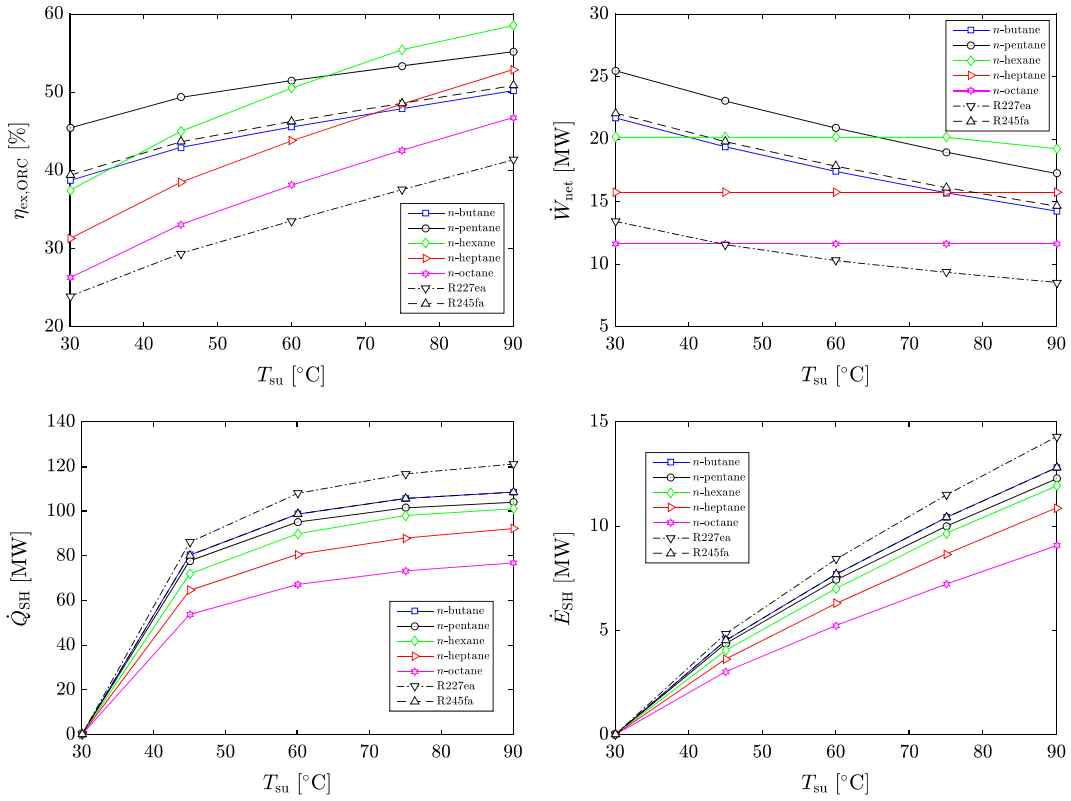

Fig. 2. ORC exergy efficiency (top left), net power output (top right), heating capacity/hot-water enthalpy difference (bottom left) and heat-demand exergy (bottom right) of the ORC-CHP system as a function of the hot-water supply temperature for selected single-component working fluids and the high-temperature ($T_{hs} = 330$ °C) heat source.

Table 1
Optimal operating conditions for the ORC-CHP system with different working-fluids for the high-temperature (T_{hs} = 330 °C) heat source and two (low/high) heat-supply temperatures.

Fluid	30 °C supply temperature						90 °C supply temperature					
	P_{evap} [bar]	P_{cond} [bar]	T_{cond} [°C]	θ_{sh} [−]	$\dot{m}_{wf}$ [kg/s]	$\dot{m}_{cs}$ [kg/s]	P_{evap} [bar]	P_{cond} [bar]	T_{cond} [°C]	$\dot{m}_{wf}$ [kg/s]	θ_{sh} [−]	$\dot{m}_{cs}$ [kg/s]
n-butane	36.1	3.41	36.3	0.317	245	3250	36.1	6.61	61.4	178	0.745	433
n-pentane	32.0	1.03	36.5	0.192	239	3160	32.0	2.65	67.5	197	0.495	415
n-hexane	28.8	1.00	68.3	0.027	238	2870	28.8	1.07	70.4	204	0.264	403
n-heptane	26.0	1.00	97.9	0.000	211	2570	26.0	1.00	97.9	211	0.000	368
n-octane	23.7	1.00	125.0	0.000	170	2140	23.7	1.00	125.0	170	0.000	306
R227ea	27.8	6.19	35.5	0.288	750	3470	27.8	8.98	49.2	404	1.000	483
R245fa	34.7	2.21	36.2	0.365	462	3250	34.7	4.86	61.8	345	0.812	433

irrespective of the hot-water supply temperature. This is because the condensation takes place at a constant pressure of 1 bar as a result of the constraint in Eq. (14). This constraint ensures that the cycle operates above atmospheric pressure, thus eliminating the need for expensive vacuum expanders and condensers. At this condensation pressure of 1 bar, the working-fluid temperature is generally greater than the cooling-water exit temperature. For example, the saturation (and condensation) temperatures of *n*-heptane and *n*-octane at 1 bar are 97.9 °C and 125.0 °C, respectively, as shown in Table 1. Thus, increasing the cooling-water exit temperature does not influence the working-fluid condensation temperature and pressure.

Although the power output is relatively insensitive to the cooling-water exit temperature for *n*-hexane, *n*-heptane, *n*-octane, the heating capacity and heat-demand exergy both increase at higher cooling-stream exit temperatures from the ORC condenser due to the increased temperature rise of this stream and its improve thermal match with the cycle at higher temperatures. This is an unexpected result, which arises due to the saturation of the power output from the ORC engine for these working fluids as explained above. Similarly, for the other working fluids, the heating capacity and heat-demand exergy both generally increase with the heat-supply temperature, as the power output decreases. Therefore, for these working fluids, the thermal output from the CHP system appears to be in competition with the ORC power output, as expected.

This trade-off between the electrical and thermal outputs is explored further in Fig. 3, where the average CHP exergy efficiency over a year is reported as a function of the heat-demand profile for selected working fluids and heat-supply temperatures. The blue/-solid and red/dashed areas in the figure represent ranges of the CHP coefficient x_{CHP} corresponding to residential and industrial energy demands according to typical heat-demand intensity values (Section 3.4, Refs. [54–56]). As expected, the CHP exergy efficiency η_{CHP} decreases at lower heat-demand intensities, and this effect is more remarkable at higher heat sink supply temperatures.

In terms of the ORC exergy efficiency, the ORC-CHP system is generally more efficient for designs with higher hot-water supply temperatures, notwithstanding the fact that the system delivers lower power-outputs at higher heat-supply temperatures. This is possible because of the higher space-heating potential available at higher heat-supply temperatures. From Fig. 2, it is clear that the space-heating exergy increases by at least 9 MW (between hot-water supply temperatures of 30 °C and 90 °C), although the net power output decreases by a maximum of about 8 MW over the same temperature range. Thus, the increase in space-heating exergy with heat-supply temperature is steeper than the decrease in net power output, leading to an overall increase in the ORC-CHP system's exergy efficiency with the hot-water supply temperature.

From Fig. 2 we can draw some conclusions concerning the performance of different working fluids in the ORC-CHP system. The refrigerants have the highest space-heating exergy followed by the *n*-alkanes; the space-heating exergy decreases progressively as the *n*-alkanes become heavier (from *n*-butane to *n*-octane). This is evident regardless of the hot-water supply temperature. While R227ea provides the largest space-heating exergy across all supply temperatures, it leads to an ORC-CHP design with the lowest exergy-efficiency due to its comparatively low power-output. Amongst the *n*-alkane working fluids, *n*-octane provides the lowest space-heating exergy and power output and thus leads to the least efficient CHP-ORC design.

Working fluids such as the *n*-alkanes *n*-butane, *n*-pentane, and *n*-hexane lead to designs with the highest power outputs, which can be in excess of 20 MW. They also have high values of space heating exergy (although slightly lower than that of R227ea) and are thus seen to exhibit the highest ORC system exergy efficiency.

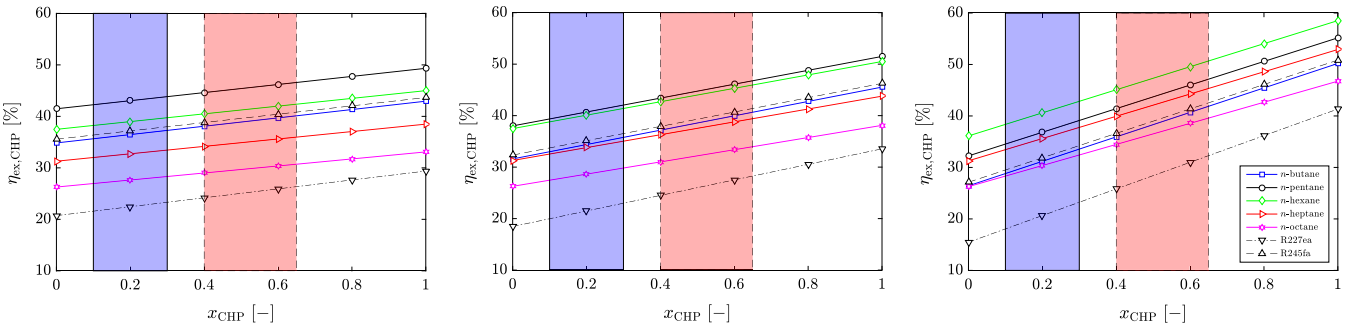

Fig. 3. CHP exergy efficiency of the ORC-CHP system as a function of the heat-demand intensity (coefficient x_{CHP} in Eq. (15)) for selected single-component working fluids, the high-temperature (T_{hs} = 330 °C) heat source and hot-water supply temperatures of 45 °C (left), 60 °C (center) and 90 °C (right). The solid/blue and dashed/red areas represent the x_{CHP} ranges of residential and industrial heat demands, respectively. (For interpretation of the references to colour in this figure legend, the reader is referred to the web version of this article.)

In particular, ORC-CHP systems with *n*-pentane as working fluid have the highest ORC exergy efficiency and net power output, up till about 65 °C, after which systems with *n*-hexane as the working fluid are the most efficient and most powerful.

4.2. Working-fluid mixture performance

Having considered using single-component organic fluids for harnessing high-temperature heat (T_{hs} = 330 °C) in an ORC-CHP system, it is interesting to consider what opportunities mixtures of such fluids offer. In ORC systems, working-fluid mixtures, due to their temperature glide during isobaric evaporation/condensation provide a better thermal match to the heat-source/sink streams thereby reducing systems' exergy losses and improving overall performance. It should be noted that working-fluid mixtures could lead to deterioration in heat transfer performance especially during evaporation and condensation. Systems with such working-fluid mixtures may thus eventually require larger heat-transfer equipment compared to those with single-component working fluids.

In this work however, we limit the analysis to the thermodynamic effect(s) of such working-fluid mixtures on the ORC-CHP system. For this reason, we simulate the ORC-CHP model with mixtures of working fluids from the *n*-alkanes and refrigerants presented earlier. Amongst the pure fluids, *n*-pentane and *n*-hexane lead to cycle designs with the highest exergy efficiencies and net power outputs. Thus, we start the investigation of working-fluid mixtures in the ORC-CHP system with a mixture of *n*-pentane and *n*-hexane. Other *n*-alkane mixtures and the refrigerant mixtures are considered and evaluated later in this section.

All performance indices of the ORC-CHP system considered in the present work with a working-fluid mixture of *n*-hexane and *n*-pentane are presented in Fig. 4; the mixtures here and hereafter, are defined on a mass fraction basis. As with the single-component working fluids, the ORC net power decreases with increasing hot-water supply temperature while the heat-demand exergy, heating capacity and the ORC exergy efficiency both increase with the hot-water supply temperature. The use of working-fluid mixtures seems to have a negligible effect on the heat-demand exergy and the heating capacity as the working-fluid mixtures only allow a small margin of improvement over the pure fluids (*n*-hexane and *n*-pentane).

In addition, the two most conventional CHP performance indicators, namely the energy utilization factor (EUF) and the fuel energy savings ratio (FESR) for the ORC-CHP system are presented, demonstrating the economic benefits of such a system in comparison to a combination of a conventional power station and a conventional boiler. At hot-water supply temperatures below 45 °C, the system is seen to have low values of EUF and negative values of FESR as low amounts of heat is generated and its electrical efficiency is generally low, lower than the 40% assumed for the conventional plant. However, at higher supply temperatures (greater than 45 °C), the ORC-CHP system is seen to perform favourably in comparison to the conventional systems with FESR values in excess of 10%. This is a result of the larger amount of heating capacity provided at the higher temperatures which also leads to higher values of the EUF. Generally, the working-fluid mixtures result in similar fuel savings as the pure working fluids in the ORC-CHP system.

As shown in Fig. 5, working-fluid mixtures allow considerable improvements to the performance of the ORC-CHP system in terms of net power output and exergy efficiency. In particular, a fluid mixture is usually seen to exhibit a higher system exergy efficiency and/or power output than its two constituent pure fluids, especially at higher hot-water supply temperatures. This benefit arises due to the non-isothermal condensation profile of the mixtures, which offers a better thermal match with the heat sink and therefore allows lower condensation pressures (and higher evaporation pressures) and leads to higher power outputs exhibited by the systems with working-fluid mixtures. It is noted that, although this will not always apply when employing mixtures since it will depend on many factors (*i.e.*, the working fluid and its constituents, temperature glide of the mixture, pinch position, heat source or sink temperature gradient), it was observably the case here when inspecting the resulting cycles. In the condenser, the pinch point usually occurs at the dew point for pure working fluids due to their isothermal condensation profile (as in Fig. 13). Here, the temperature difference between the working fluid and the cooling stream is at the minimum of 10 °C (from Eq. (12)); elsewhere along the condenser, the temperature difference is greater than this minimum. When a working-fluid mixture is employed, the condensation is non-isothermal and the resulting glide on condensing relaxes the pinch from the dew point and hence the temperature difference between the working fluid and the cooling stream along the condenser, is greater than the minimum. This enables the condensation pressure to be lowered until the pinch is re-established at some point along the condenser, in a bid to maximize the power output or the exergy efficiency of the cycle.

Furthermore, the better thermal match between the working-fluid mixture and the heat source/sink (compared to pure working fluids) also minimizes the average temperature difference between the working fluid and the heat source/sink, offering a reduction in the exergy destruction in the evaporator/condenser and thereby leading to higher exergy efficiency. The optimal composition that maximizes both the power output and the net exergy efficiency however varies with the hot-water supply temperature (and the temperature gradient of the cooling water stream). At the lowest hot-water supply temperature of 30 °C, *n*-pentane (*i.e.*, mass fraction of 1) is the optimal working fluid and at the highest temperature, *n*-hexane (mass fraction of 0) is optimal. At other supply temperatures, the optimal *n*-pentane composition varies progressively between 1 and 0, with a value of 0.5 for a hot-water supply temperature of 60 °C, further illustrating the crossover in optimal single-component working fluid from *n*-pentane to *n*-hexane as seen in Fig. 2.

Other working-fluid mixtures were also investigated for use in the ORC-CHP system; these results are presented in Fig. 5, further illustrating the performance improvements presented by working-fluid mixtures over the pure fluids in ORC-CHP systems. However, it is not in all the cases that the working-fluid mixtures perform better than their constituent pure fluids. Cycle performance with R227ea + R245fa mixtures and *n*-butane + *n*-pentane mixtures are seen to be no better than those with pure R245fa and pure *n*-pentane respectively; the ORC exergy efficiency only varies linearly between the constituent pure fluids and are thus excluded from Fig. 5. In addition, for most of the mixtures at a hot-water supply temperature of 30 °C, the exergy efficiency varies linearly between the constituent pure fluids with no mixing ratio posing a better alternative to the pure fluids. Only the working-fluid mixture of *n*-butane + *n*-hexane gives a better performance over the pure fluids, with a mixture having a *n*-hexane mass fraction of 0.8 maximizing the ORC exergy efficiency.

It can be seen from Fig. 5 that at higher hot-water supply temperatures a larger number of working-fluid mixtures deliver an improved performance over their constituent pure fluids. This improvement attained by the mixtures is facilitated by the cooling water stream temperature profile, which is now better matched to the working fluid condensation temperature profile. In particular, for a hot-water supply temperature of 60 °C working-fluid mixtures with 20% *n*-butane + 80% *n*-hexane and all three mixtures featuring *n*-pentane (50% *n*-hexane + 50% *n*-pentane, 20% *n*-heptane + 80% *n*-pentane and 20% *n*-octane + 80% *n*-pentane) maximize the ORC exergy efficiency and perform better than their

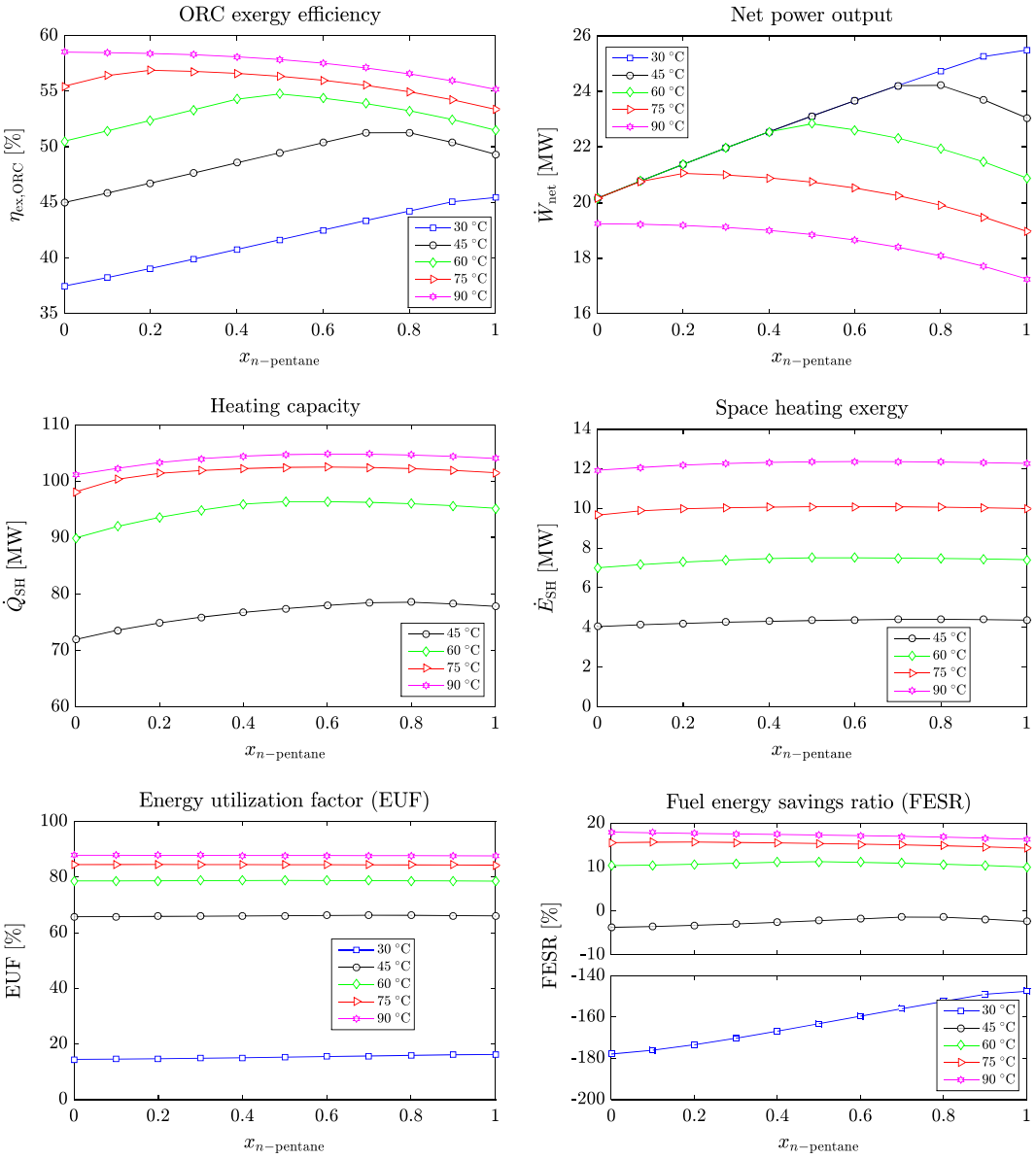

Fig. 4. ORC exergy efficiency (top left), net power output (top right), heating capacity/hot-water enthalpy difference (middle left), heating exergy (middle right), energy utilization factor (EUF, bottom left) and fuel energy savings ratio (FESR, bottom right) of the ORC-CHP system for *n*-hexane + *n*-pentane working-fluid mixtures, the high-temperature (T_{hs} = 330 °C) heat source and hot-water supply temperatures of 45 °C, 60 °C, 75 °C and 90 °C.

constituents (pure *n*-butane, *n*-pentane, *n*-hexane, *n*-heptane and *n*-octane).

The performance improvement achieved by employing working-fluid mixtures is even more noticeable at a hot-water supply temperature of 90 °C, especially for working-fluid mixtures containing *n*-pentane and *n*-heptane or *n*-octane, as the temperature profile of the cooling stream and the condensing working fluid become better matched. The mixtures of *n*-octane + *n*-pentane generally have the largest temperature glide and are thus better matched to the heat sink, resulting in a maximum exergy efficiency at a *n*-pentane mass fraction of 0.7. The mixtures with *n*-hexane (with *n*-heptane and *n*-octane as the second constituent) perform less well than those with *n*-pentane because they have lower temperature glides and are not as good as a match with the cooling stream as do the working-fluid mixtures with *n*-pentane as a constituent.

If the low temperature heat-demand profile is taken into account and the coefficient x_{CHP} is ranged between 0 and 1, the CHP exergy efficiency values of Fig. 6 are obtained, for the different working-fluid mixtures and heat sink temperatures of 90 °C to 60 °C.

4.3. Performance with medium- and low-temperature heat sources

Having discussed the use of single-component and mixture ORC working fluids for high heat source temperatures, we proceed now to consider optimal working-fluid mixtures for lower heat-source temperatures, in particular 250 °C (medium temperature) and 150 °C (low temperature). For the medium-temperature heat source, its mass flow rate is considered to be 120 kg/s, while for the low-temperature heat source, the mass flow rate is set to 30 kg/s.

Fig. 7 shows exergy efficiencies for different working-fluid mixtures and hot-water supply temperatures. The same fluid mixtures are considered as for the high temperature heat-source, along with *n*-butane + *n*-pentane mixtures; R227ea + R245fa mixtures are

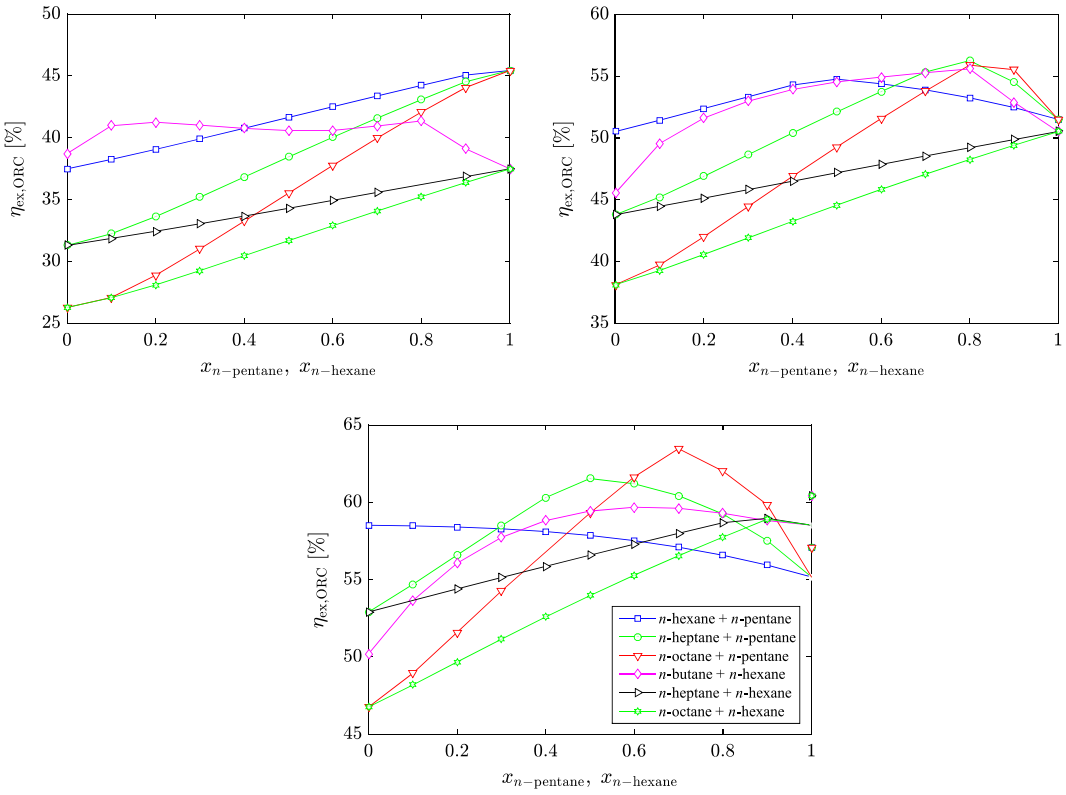

Fig. 5. ORC exergy efficiency of the ORC-CHP system for selected working-fluid mixtures, the high-temperature (T_{hs} = 330 °C) heat source and hot-water supply temperatures of 30 °C (top left), 60 °C (top right) and 90 °C (bottom). The horizontal axes are defined in terms of the composition of the second fluid listed in each of the fluid combinations, *i.e.*, *n*-pentane and *n*-hexane, respectively. For the *n*-pentane + *n*-hexane mixtures, results are displayed with respect to the mass fraction of *n*-pentane on the horizontal axes.

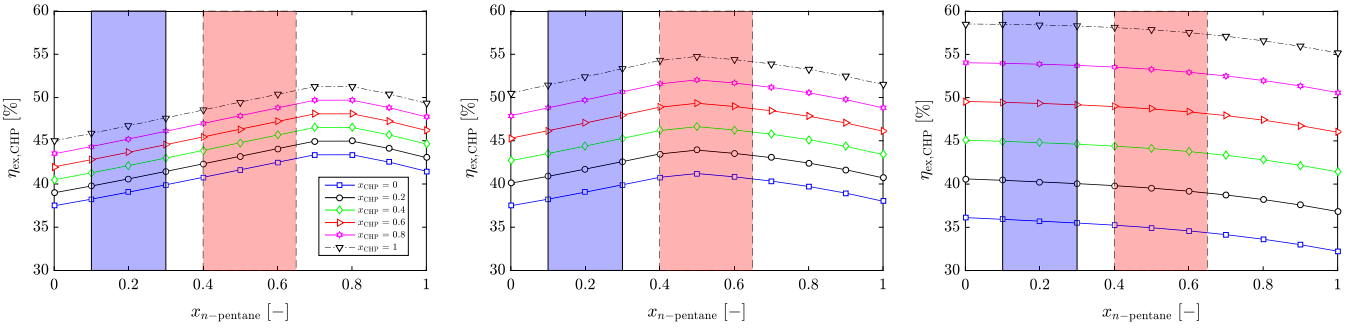

Fig. 6. CHP exergy efficiency of the ORC-CHP system for *n*-hexane + *n*-pentane working-fluid mixtures, different heat-demand intensities (coefficient x_{CHP} in Eq. (15)), the high-temperature (T_{hs} = 330 °C) heat source and hot-water supply temperatures of 45 °C (left), 60 °C (center) and 90 °C (right). The solid/blue and dashed/red areas represent the x_{CHP} ranges of residential and industrial heat demands, respectively. (For interpretation of the references to colour in this figure legend, the reader is referred to the web version of this article.)

excluded here since these only show a linear increase with increasing R245fa concentration in the mixture. For a hot-water supply temperature of 30 °C, the ORC exergy efficiency ranges between 22% and 55%, for 60 °C between 35% and 62%, and for 90 °C between 44% and 63%. Thus, the exergy efficiency increases in general with higher hot-water supply temperatures as the heat that is available for space heating increases. At the same time, the power output decreases at higher hot-water temperatures, however, this is less pronounced than the increase in space heating exergy giving a higher exergy efficiency.

In particular, for a low hot-water supply temperature of 30 °C, a 20% *n*-butane + 80% *n*-pentane working-fluid mixture is associated with the highest ORC exergy efficiency at 52.1%, which is marginally higher than the exergy efficiency of pure *n*-pentane at 51.9%. For a supply temperature of 60 °C, the best performing mixture is 60% *n*-butane + 40% *n*-hexane with an exergy efficiency of 62.0%. Finally, for the higher supply temperature of 90 °C, the mixture of 80% *n*-pentane + 20% *n*-octane has the highest ORC exergy efficiency at 62.7%. Thus, at higher heat supply temperatures mixtures consisting of molecules with longer chains perform better.

Fig. 8 shows the CHP efficiencies for selected values of x_{CHP}, which takes into account the heat demand (see Eq. (15)), when using *n*-butane + *n*-pentane mixtures and hot-water supply temperatures of 45 °C, 60 °C and 90 °C. A unity value for x_{CHP} (= 1) represents a heat demand of 100%, *i.e.,* heat is required during the entire operation of the CHP engine, whereas for x_{CHP} = 0 no heat is required throughout the year, and thus only the generated net power contributes to the CHP efficiency. For a hot-water supply temperature of 30 °C the space heating exergy is 0, which means that no demand for space heating can be satisfied. For the case of

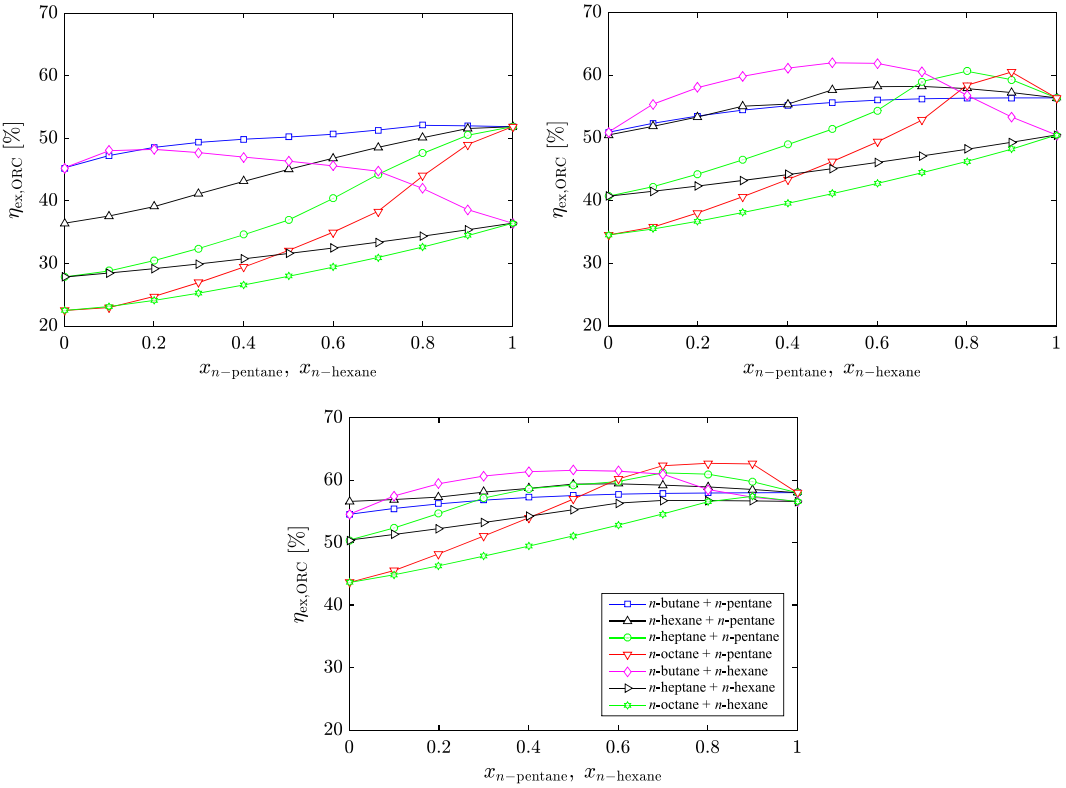

Fig. 7. ORC exergy efficiency of the ORC-CHP system for selected working-fluid mixtures, the medium-temperature (250 °C) heat source and hot-water supply temperatures of 30 °C (top left), 60 °C (top right) and 90 °C (bottom). The horizontal axes are defined in terms of the composition of the second fluid listed in each of the fluid combinations, *i.e.*, *n*-pentane and *n*-hexane, respectively. For the *n*-pentane + *n*-hexane mixtures, the results are displayed with respect to the mass fraction of *n*-pentane on the horizontal axes.

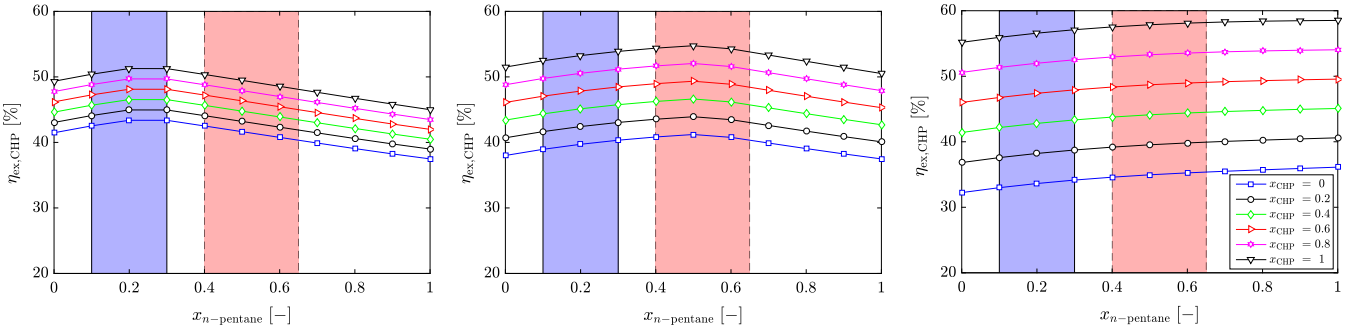

Fig. 8. CHP exergy efficiency of the ORC-CHP system for *n*-butane + *n*-pentane working-fluid mixtures, different heat-demand intensities (coefficient x_{CHP} in Eq. (15)), the medium-temperature (250 °C) heat source and hot-water supply temperatures of 45 °C (left), 60 °C (center) and 90 °C (right). The solid/blue and dashed/red areas represent the x_{CHP} ranges of residential and industrial heat demands, respectively.

T_{su} = 30 °C (and x_{CHP} = 0), the engine's CHP efficiency is identical to its thermal efficiency and is not considered in Fig. 9. In case of x_{CHP} = 1, the CHP efficiency corresponds to the exergy efficiency from Fig. 8.

From Fig. 8 it can be seen that for each respective hot-water supply temperature, the CHP efficiency increases for increasing values of x_{CHP}, *i.e.*, for longer heat-demand periods. This is due to the higher usage of the space heating exergy for increasing values of x_{CHP}, which would be a loss for values of x_{CHP} smaller than 1. In case of a hot-water supply temperature of 90 °C the CHP efficiency for x_{CHP} = 1, is higher than for a supply temperature of 45 °C. The CHP efficiency is lower in case of a hot-water supply temperature of 90 °C for x_{CHP} = 0, than it is for a supply temperature of 45 °C. This means that for heat demands in the domestic sector (blue column in Fig. 9) a hot-water supply temperature of 45 °C has the highest CHP efficiency with a mixture of 20% *n*-pentane + 80% *n*-butane. For the industrial sector, a hot-water supply temperature of 60 °C using the mixture of 50% *n*-pentane + 50% *n*-butane has the highest CHP efficiency at x_{CHP} = 0.4 and a hot-water supply temperature of 90 °C using pure *n*-butane for x_{CHP} = 0.6.

Fig. 9 shows the ORC exergy efficiencies for various working-fluid mixtures for a heat source temperature of 150 °C and hot-water supply temperatures of 30 °C, 60 °C and 90 °C, respectively. As is the case with the high and medium temperature heat-sources, the R227ea + R245fa mixture is excluded from the plots. Similar to the results for the medium temperature heat-source (Fig. 8) the exergy efficiency increases with increasing hot-water supply temperatures. Further, the single mixtures have more similar exergy efficiencies for higher supply temperatures. Especially the mixtures that have constituents with similar chain lengths

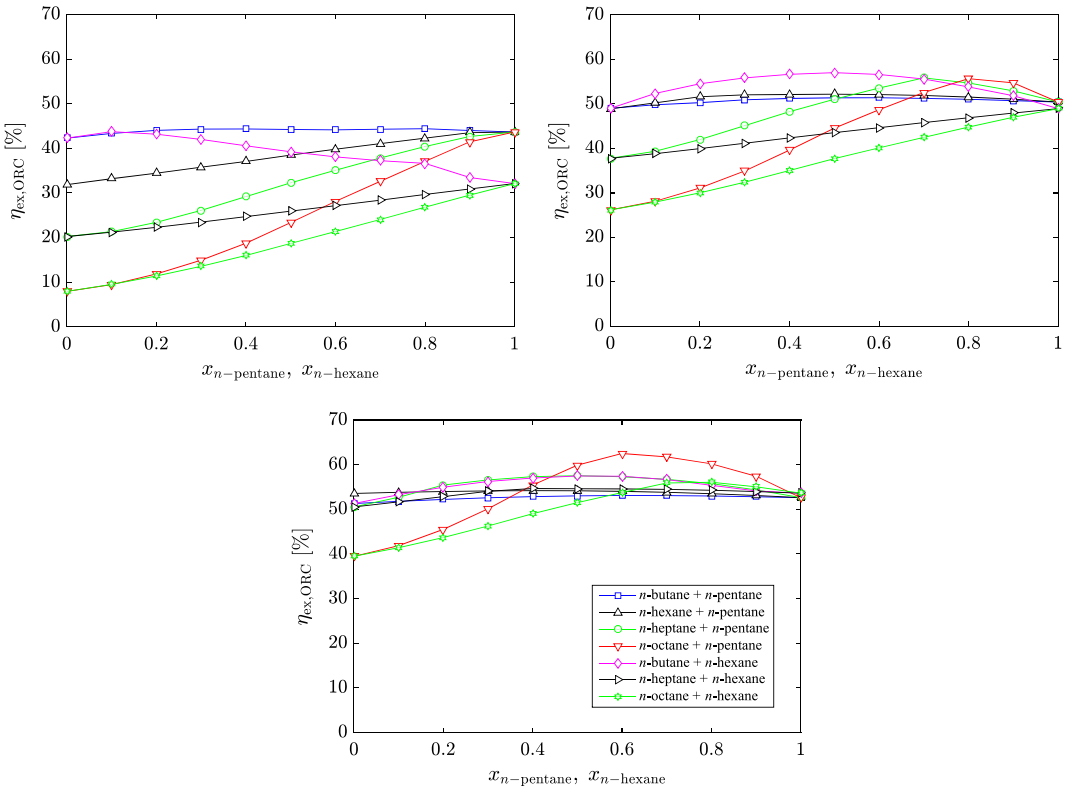

Fig. 9. ORC exergy efficiency of the ORC-CHP system for selected working-fluid mixtures, the low-temperature (150 °C) heat source and hot-water supply temperatures of 30 °C (top left), 60 °C (top right) and 90 °C (bottom). The horizontal axes are defined in terms of the composition of the second fluid listed in each of the fluid combinations, *i.e.*, *n*-pentane and *n*-hexane, respectively. For the *n*-pentane + *n*-hexane mixtures, the results are displayed with respect to the mass fraction of *n*-pentane on the horizontal axes.

(*n*-butane + *n*-pentane, *n*-pentane + *n*-hexane, *n*-hexane + *n*-heptane) have very similar exergy efficiencies that are almost constant over the entire composition range. This is due to the pure components (*n*-butane, *n*-heptane, *n*-hexane and *n*-heptane) having very similar efficiencies (approx. 50%) for hot-water supply temperatures of 90 °C, whereas for supply temperatures of 30 °C the exergy efficiencies of those pure components vary between 8% and 42% and for supply temperatures of 60 °C between 27% and 50%.

The CHP efficiencies for *n*-butane + *n*-pentane mixtures at hot-water supply temperatures of 45 °C, 60 °C and 90 °C for various values of x_{CHP} are shown in Fig. 10. As it could be seen in Fig. 9 for a heat source temperature of 250 °C, the CHP efficiency increases with increasing heat demand. Furthermore, for $x_{CHP} = 1$, the CHP efficiency increases with increasing hot-water supply temperature, while the CHP efficiency stays almost constant for $x_{CHP} = 0.8$ and decreases for lower values of x_{CHP} with increasing hot-water supply temperatures. For the domestic sector with heat demands of $0.15 \leq x_{CHP} \leq 0.30$ the highest CHP efficiency can be achieved with a hot-water supply temperature of 45 °C and a mixture of 60% *n*-pentane + 40% *n*-butane. In the industrial sector, where the heat demand is typically in the range $0.40 \leq x_{CHP} \leq 0.65$, the highest CHP efficiency is achieved by a 50% *n*-pentane + 50% *n*-butane mixture at a hot-water supply temperature of 45 °C.

As with the high-temperature heat source case in Fig. 4, the fuel energy savings ratio (FESR) and the energy utilization factor (EUF) of the ORC-CHP system are presented for the medium- and low-temperature temperature heat sources in Fig. 11. Due to the low amount of heat generated at supply temperatures below 45 °C (and none at 30 °C), the FESR of the ORC-CHP system is negative at these temperatures; similarly, the EUF values are quite low. When larger amounts of heat is supplied by the system (at supply

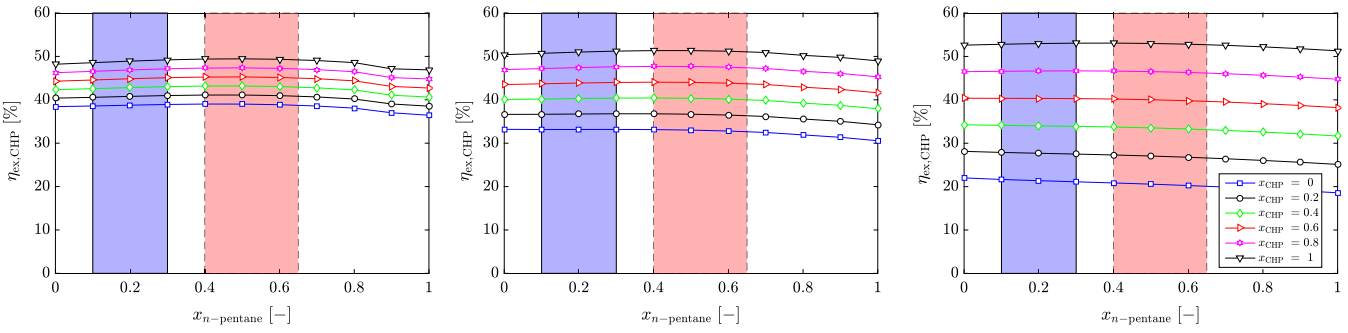

Fig. 10. CHP exergy efficiency of the ORC-CHP system for *n*-butane + *n*-pentane working-fluid mixtures, different heat-demand intensities (coefficient x_{CHP} in Eq. (15)), the low-temperature (150 °C) heat source and hot-water supply temperatures 45 °C (left), 60 °C (center) and 90 °C (right). The solid/blue and dashed/red areas represent the x_{CHP} ranges of residential and industrial heat demands, respectively.

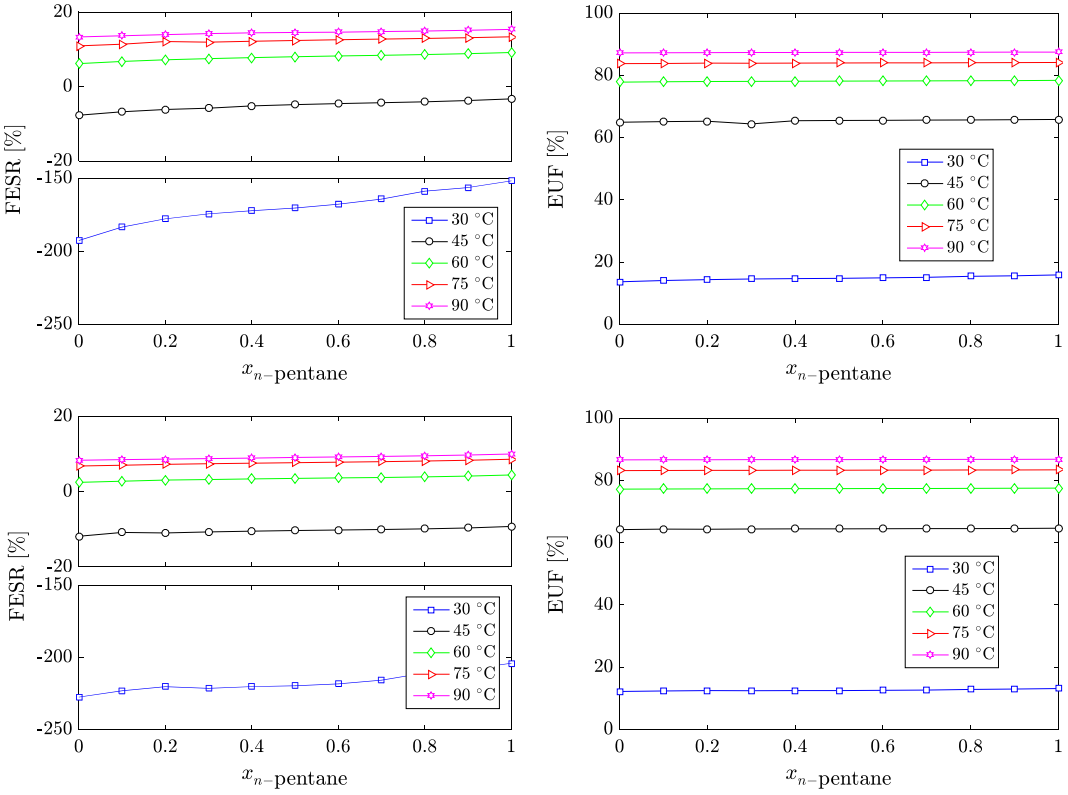

Fig. 11. FESR and EUF of the ORC-CHP system for *n*-butane + *n*-pentane working-fluid mixtures at the medium-temperature heat source (250 °C, top) and at the low-temperature heat source (150 °C, bottom), at hot-water supply temperatures of 45 °C, 60 °C, 75 °C and 90 °C. At 30 °C, there is no hot-water supply and the system operates in electricity mode.

temperatures of 60 °C and above), the system is seen to generate positive fuel savings with FESR values approaching 20% and EUF values approaching 90%. Similarly to the CHP exergy efficiency, the FESR and EUF of the ORC-CHP system are rather insensitive to the composition of the working-fluid mixture.

4.4. Overall CHP exergy efficiency and optimal working-fluid selection

Overall, the CHP efficiency of the ORC engine is a complex function of the engine design, hot-water supply temperature and selected working-fluid (or mixture), the market energy-demand segment (x_{CHP}), and the waste-heat source characteristics (temperature and energy content). Thus, the question arises as to what engine design (and working fluid) would maximize its CHP exergy efficiency. This is approached by evaluating the performance of the aforementioned pure working fluids and their mixtures in the ORC-CHP engine, with the objective of maximizing the engine's CHP exergy efficiency. The optimal working-fluid mixtures at different hot-water supply temperatures (45 °C, 60 °C and 90 °C) and for different ranges of the energy demand are presented in Table 2, with the corresponding CHP efficiency values plotted in Fig. 12, for the three waste-heat sources discussed earlier (150 °C, 250 °C and 330 °C).

The optimal working fluids (as presented in Table 2) are generally hydrocarbon mixtures, usually those of either *n*-pentane or *n*-hexane mixed with other *n*-alkanes. Another key characteristic of these working fluids is that they predominantly feature a high concentration of either *n*-pentane or *n*-hexane. This is partly due to the fact that *n*-pentane and *n*-hexane are the two most efficient pure working fluids (highest CHP efficiencies in Fig. 4) and also that their mixtures are better matched to the heat source/sink streams. From Table 2, it is clear that the optimal working fluid varies with the heat-demand segment, especially for the low- and medium-temperature heat source; for the high-temperature heat source, the optimal working fluid is constant across the heat-demand segment and only varies with the hot-water supply temperature. The optimal CHP efficiency also varies widely (from 30% to over 60%) with the heat demand.

At low values of heat demand, the engine has lower CHP efficiencies at high hot-water supply temperatures. This is due to the low utilization (or zero utilization when $x_{CHP} = 0$) of the high (or low) quality heat available. Moreover, at these low energy demand segments, the CHP efficiency is dominated by the electric power such that when $x_{CHP} = 0$, the CHP efficiency is a direct measure of the electrical thermal efficiency. At demand segments ranging between 30% and 70% and above, the designs with the high hot-water supply temperatures become more efficient; this description holds for the three heat-source cases considered, as illustrated in Fig. 12. At high heat demands ($0.6 < x_{CHP} < 1$), the engine designs with higher hot-water supply temperatures become more efficient due to the high (or complete, at $x_{CHP} = 1$) utilization of the higher quality heat available.

Thus, for a high heat-demand user, it is be more profitable to design the ORC-CHP system to generate a large amount of high-quality heat, *i.e.*, hot-water supply temperatures of 90 °C or higher. On the other hand, for low heat demands, it is more profitable to design it for maximum power generation, corresponding to low hot-water supply temperatures (below 45 °C). Furthermore, since the optimal working-fluid mixture remains constant (especially for a high-temperature heat source), one system can be designed (with a fixed working fluid) to suitably meet and satisfy the varying levels of heat demand at different times of the year. This can be made possible by enabling a facility to vary the flowrate of the cooling water through the system as appropriate – a high flowrate

Table 2
The optimal working-fluid mixture, for each case study (low-, medium- and high-temperature heat source) and energy demand market segment (*i.e.*, temperature of hot-water supply at 45 °C, 60 °C, 90 °C, and CHP demand intensity coefficient, χ_{CHP}). The corresponding global (maximum) CHP efficiency values are given in Fig. 12. The mass fractions of each of the working fluid components are given in parentheses.

Heat source temperature	Hot water supply temperature	Heat-demand intensity (χ_{CHP}) range				
		0–0.2	0.2–0.4	0.4–0.6	0.6–0.8	0.8–1
Low (150 °C)	45 °C	*n*-heptane (0.3) + *n*-pentane (0.7)	*n*-octane (0.1) + *n*-pentane (0.9)		*n*-butane (0.5) + *n*-hexane (0.5)	*n*-butane (0.7) + *n*-hexane (0.3)
	60 °C		*n*-butane (0.6) + *n*-hexane (0.4)			
	90 °C		*n*-octane (0.3) + *n*-pentane (0.7)		*n*-octane (0.4) + *n*-pentane (0.6)	
Medium (250 °C)	45 °C	*n*-butane (0.4) + *n*-hexane (0.6)	*n*-heptane (0.1) + *n*-pentane (0.9)		*n*-butane (0.5) + *n*-hexane (0.5)	
	60 °C					
	90 °C		*n*-octane (0.2) + *n*-pentane (0.8)			
High (330 °C)	45 °C	*n*-heptane (0.1) + *n*-pentane (0.9)				
	60 °C	*n*-heptane (0.2) + *n*-pentane (0.8)				
	90 °C	*n*-octane (0.3) + *n*-pentane (0.7)				

can be used to generate low-temperature hot water for periods of low heat demand, whereas the flowrate can be reduced to generate hot water at higher temperatures for the periods of high heat demand.

4.5. Further efficiency improvements via heat recovery

Aside from the power production from the working-fluid expansion and the space heating provided by the low-temperature cooling water exiting the ORC condenser, additional useful thermal energy (and, therefore, exergy) can be recovered from the heat-source stream after it exits the evaporator. This amount of useful exergy is a direct function of the temperature of the heat source exiting the evaporator ($T_{hs,exit}$) and also its mass flow rate. Indirectly, it is a function of the cycle configuration (working-fluid mass flow rate, evaporation/condensation pressures, degree of superheat), the net power production of the cycle and the amount of heat extracted from the heat source (for subsequent conversion to power); the higher the heat extracted from the heat source, the lower its eventual exit temperature and *vice versa*.

The combinations of these factors that lead to a high-power cycle (typically, high working-fluid mass flowrate, evaporation pressures, degree of superheat, and low condensation pressures) will generally lead to a lower heat-source exit temperature, as more heat will be extracted from the heat source for conversion in the cycle. This implies that designing cycles to maximize exergy (one should note that the exergy is dominated by the net electrical power output as illustrated in Figs. 2 and 4) will inherently lead to low heat-source exit temperatures. Nonetheless, this exit stream could still possess some potential for useful work, especially for purposes of further space heating, thereby reducing the exit temperature to the barest possible minimum.

Ideally, the highest benefit will be derived by extracting the maximum possible amount of heat from the heat source, thereby reducing its exit temperature to that of the environment (~20 °C). However, the exit temperature of the heat source can be limited by its acid dew point temperature. Below this temperature, gaseous acids in the gas will condense, leading to a high possibility of corrosion. Thus, it is detrimental (and not economical) to further extract heat from the source once this temperature is approached. For the heat sources considered in this work, the flue gas acid dew point varies between 42 °C and 75 °C. Using the upper limit of 75 °C, the additional heat recovery potential of the flue gas exiting the evaporator can be calculated. The values for different cycle configurations are presented in Table 3, where the average heat-source exit temperatures ($T_{hs,exit}$) are also provided for the three heat sources and the different levels of hot-water supply temperature.

The heat-source exit temperatures are lowest for the high-temperature heat source and highest for the low-temperature heat source; one might have expected the reverse to be the case. The temperature enthalpy (T–$\dot{Q}$) diagrams of three cycle configurations (with *n*-pentane as the working fluid) with the three heat sources are presented in Fig. 13. These diagrams provide a visualization of the heat addition processes in these cycles, from which the relationship between the heat-source streams and the working-fluid can be explored.

The low-temperature (150 °C) heat source causes the working fluid to be evaporated at a lower evaporation temperature/pressure where the phase-change enthalpy is higher (than at a higher evaporation temperature/pressure). As illustrated in Fig. 13, the phase change enthalpy is roughly equal to the enthalpy required to heat the working fluid to its bubble point. This, combined with the low temperature of the heat source, causes the pinch point to occur at the onset of evaporation (*i.e.*, the bubble point, and leading

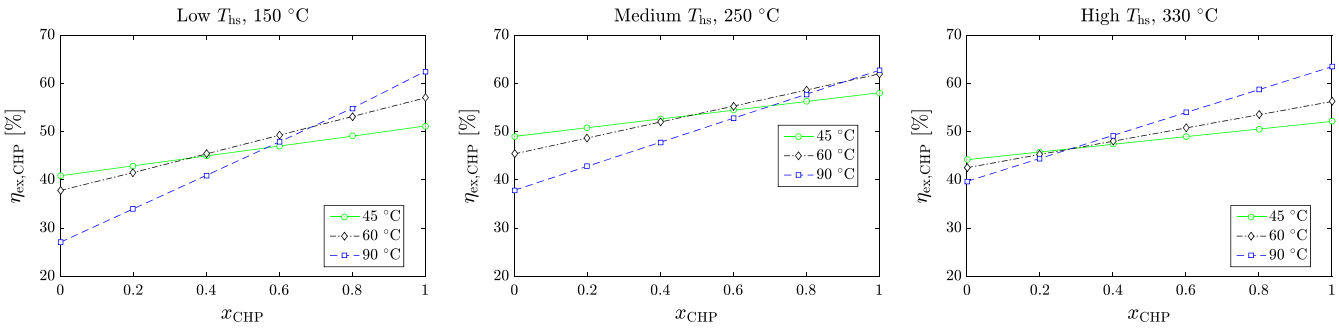

Fig. 12. The global (maximum) CHP efficiency for each case study (LHS: low-temperature heat source, middle: medium-temperature heat source, RHS: high-temperature heat source) and energy demand market segment (*i.e.*, temperature of hot-water supply at 45 °C, 60 °C, 90 °C, and CHP demand intensity coefficient, x_{CHP}). The corresponding optimal working-fluid mixtures are given in Table 2.

Table 3
Average ORC-CHP system/evaporator exit temperatures and additional heat recovery potentials from the heat-source streams (at entry temperatures of 150 °C, 250 °C and 330 °C) exiting the evaporator and serving different hot-water supply temperatures (T_{su}).

T_{su} (°C)	Average heat-source exit temperature (°C)			Heat recovery potential (MW)		
	150 °C	250 °C	330 °C	150 °C	250 °C	330 °C
30	137	108	75.9	1.85	3.97	0.48
45	138	107	80.1	1.88	3.86	2.87
60	138	109	83.8	1.90	4.12	4.92
75	139	114	87.6	1.93	4.64	7.08
90	140	120	92.1	1.96	5.34	9.59

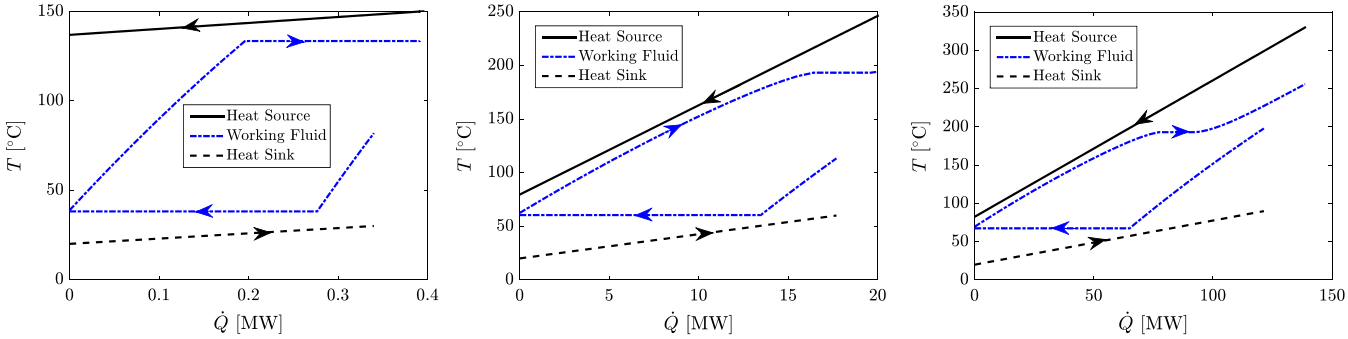

Fig. 13. Temperature-enthalpy (T–$\dot{Q}$) diagrams of the ORC working fluid and heat source/sink streams with n-pentane as the working fluid and (left) the low-temperature (150 °C) heat source and hot-water supply at 30 °C, (center) the medium-temperature (250 °C) heat source and hot-water supply at 60 °C, and (right) the high-temperature (330 °C) heat source and hot-water supply at 90 °C.

to the fairly gradual profile of the heat source), thereby restricting the amount of heat that can be extracted from the heat source and its eventual temperature drop. Thus, there is only about a 10 °C to 15 °C temperature drop for the heat source.

Conversely, for medium- and high-temperature heat sources, the elevated heat source temperatures allow the working fluid to be evaporated at higher pressures/temperatures where the enthalpy of vaporization is a smaller fraction of the enthalpy required to get the fluid to its bubble point. Thus, for these cases, the pinch point does not occur at the bubble point, but at a lower temperature which allows the heat-source to have a steeper slope on the T–$\dot{Q}$ diagram. This is also enabled by the higher heat-source temperatures and the presence of a considerable amount of superheating for the high-temperature heat source case. These culminate in the lower exit temperatures experienced for these heat sources in comparison with the low-temperature heat source.

The heat recovery potential from the heat sources exiting the evaporator are also presented in Table 3 where the low-temperature heat source generally has the lowest potential and the high-temperature heat source has the highest where up to 9 MW can be recovered. Although the amount of recoverable heat is small in comparison to the net power output from the cycle and the space-heating exergy provided by the cooling water, this potential can be used towards space heating or to satisfy process heating requirements in the plant, leading to an increase in the overall energy efficiency of the ORC system and the process plant. This can also prove to be very beneficial for existing plants by retrofitting the designs to take advantage of the heat content of this stream.

An ORC-CHP configuration that can utilize this exit enthalpy of the heat source is one in which it is used to provide further space heating. In this arrangement, the hot water is preheated to an intermediate temperature between the cooling water supply temperature (20 °C) and the target hot water supply temperature (30, 45, 60, 75, 90 °C) by the heat rejected in the ORC condenser. It then passes through an additional heat exchanger downstream of the

Table 4
Percentage point increases in ORC exergy efficiency ($\eta_{ex,ORC}$) derived from the reconfigured ORC-CHP system operating with the low-temperature heat source (150 °C), at a hot-water supply temperature of 90 °C and different working-fluid mixtures. The mass fractions (second row) of *n*-pentane and *n*-hexane in the mixtures are given; for the *n*-hexane + *n*-pentane mixtures, the results are displayed with respect to the mass fraction of *n*-pentane. The intermediate temperatures of the hot water stream are also provided.

	$\Delta\eta_{ex,ORC}$ (% point)						Intermediate temperature (°C)					
Mixture	0	0.2	0.4	0.6	0.8	1	0	0.2	0.4	0.6	0.8	1
n-butane + *n*-pentane	7.5	7.8	7.7	7.4	7.0	6.1	56	58	58	58	57	55
n-hexane + *n*-pentane	2.7	5.4	6.1	6.2	6.3	6.1	62	58	57	57	56	55
n-heptane + *n*-pentane	0.0	0.0	1.9	6.1	6.9	6.1	90	90	67	65	60	55
n-octane + *n*-pentane	3.0	1.9	0.0	0.0	4.0	6.1	30	57	90	88	65	55
n-butane + *n*-hexane	7.5	8.2	7.9	7.4	7.5	2.7	56	62	63	64	63	62
n-heptane + *n*-hexane	0.0	0.0	0.1	0.5	0.7	2.7	90	90	88	82	77	62
n-octane + *n*-hexane	3.0	1.5	0.0	0.0	0.6	2.7	30	42	90	90	86	62

ORC evaporator where it extracts (additional) heat from the heat source, thereby raising its temperature from the aforementioned intermediate temperature to the target supply temperature. Thus, there exists a possibility of optimizing the ORC-CHP system, with this intermediate temperature as an additional decision variable, in order to improve the overall exergy efficiency of the ORC-CHP configuration.

This configuration is investigated here for the three heat sources and the specified hot-water supply temperatures. In this optimization problem, the minimum temperature difference in the additional heat exchanger is set to 10 °C, while the temperature of the heat source exiting this heat exchanger is constrained to a minimum of 75 °C (the dew point). For the medium-temperature (250 °C) and high-temperature (330 °C) heat sources, the heat source stream already exits the evaporator at very low temperature (see Fig. 13), thus the reconfigured ORC-CHP system returns the same result as that previously investigated in Sections 4.2 and 4.3. Therefore, the intermediate temperature is generally equal to the hot-water supply temperature, the heat duty of the additional heat exchanger is essentially zero and no additional heat is extracted from these heat sources.

However, for the case of the low-temperature (150 °C) heat source, the additional heat exchanger in the reconfigured system is able to extract valuable heat from the heat source exiting the evaporator due to its higher temperature (Fig. 13). This benefit is more evident for the cases with high hot-water supply temperatures (75 °C and 90 °C). The increase in the ORC exergy efficiency when compared to the initial system configuration (see Fig. 9) is provided in Table 4 for a number of working fluids and for the 90 °C hot-water supply case; the intermediate temperatures are also provided. From Table 4, it is only in a few instances (*e.g.*, mixtures with high *n*-heptane content) that there is little or no improvement; most of the working fluids show an improvement, up to 8% points for *n*-butane + *n*-hexane, with this configuration. Thus, for ORC-CHP systems with low heat source temperatures and in which high hot-water supply temperatures are desired, this alternative configuration is worth investigating.

5. Conclusions

The aim of the present study has been to evaluate the performance of working-fluid mixtures in an organic Rankine cycle – combined heat and power (ORC-CHP) system capable of recovering and utilizing waste-heat from industrial processes. In order to explore a range of different waste-heat sources for the ORC-CHP system of interest, three typical flue gas waste-heat streams have been considered in this work. The flue-gas streams have temperatures of 150 °C, 250 °C and 330 °C, with mass flow-rates of 30 kg/s, 120 kg/s and 560 kg/s, respectively. Power is generated in such a system by the expansion of the working fluid through the ORC expander/turbine, while low-temperature cogenerated heat in the form of a hot-water stream is also provided by utilizing the cooling water exiting the ORC condenser. Straight-chained *n*-alkanes from *n*-butane to *n*-octane and the refrigerants R245fa and R227ea have been considered as ORC working fluids. Working-fluid mixtures have also been subsequently derived from these pure substances, and these have also been considered for use in the system of interest.

The performance of the investigated ORC-CHP systems has been quantified in terms of: (i) the net power-output from the ORC engine, (ii) the heat energy and heat-demand exergy available in the cooling-water stream (hot-water covering the heat demand) exiting the ORC condenser, (iii) the energy utilization factor (EUF) and fuel energy savings ratio (FESR), and (iv) two exergy efficiency measures, one concerned with the performance of the ORC engine in isolation and one considering the global performance of the CHP system while accounting explicitly for the use of the generated heat by the end user. The latter second law performance indicator, referred to as the CHP exergy efficiency, was quantified as a function of a CHP coefficient representative of the rate of useful heat delivered to the demand, *i.e.*, of the energy demand profile (residential *vs.* industrial).

The novelty of the paper arises from focusing on large-scale (up to 26 MWel) waste-heat recovery applications from flue-gas streams over a wide range of temperatures from low (150 °C) to high (up to 330 °C) aimed at supplying heat (up to 10 MWth) over a range of heat-supply temperatures from as low as 30 °C up to 90 °C, *e.g.*, aimed at district heating networks, while posing and solving a formal optimization problem for identifying optimal working-fluid mixtures that have not been previously examined in this context. Furthermore, power/heat performance trade-offs are considered explicitly based on multiple indicators from the point of view of different end-users, in the presence of temporal heat demand variations and resulting mismatches between heat generation and consumption.

The results indicate that the net power-output and the heat-demand exergy are generally competing objectives, with the heat-demand exergy increasing and the power output decreasing when the heat-demand temperature is higher within a range of temperatures from 30 °C to 90 °C. The optimal ORC shaft-power outputs vary considerably between 9 MW and 26 MW, depending on the hot-water supply temperature and working-fluid (or mixture) selected. It is found, however, that the ORC exergy efficiency increases with the hot-water supply temperature. Amongst the single-component working fluids, *n*-pentane and *n*-hexane emerge as the optimal fluids, leading to ORC-CHP system designs with the highest net power-outputs and highest exergy-efficiencies. In addition, the ORC-CHP system is seen to be more economical than conventional provision from power stations and gas boilers, with FESR values in excess of 10% achieved.

Although employing working-fluid mixtures leads to only marginal changes to the heating exergy, this decision exerts a considerable influence on the power output and exergy efficiency of the system. While the pure fluids (especially *n*-pentane) show best performance at low hot-water supply temperatures due to the small temperature increase of the cooling stream (this providing a better match with the pure fluid condensation profile than that of the mixtures), designs featuring fluid mixtures can deliver higher power outputs and exergy efficiencies at higher hot-water supply temperatures. This is especially true for mixtures with condensation temperature glides matching that of the heat sink as in the case of *n*-pentane + *n*-octane working-fluid mixtures, which are shown to be optimal at a high hot-water supply temperature of 90 °C. In particular, the working-fluid mixture of 70% *n*-octane + 30% *n*-pentane results in an ORC-CHP system with the highest ORC exergy efficiency of 63% when utilizing 330 °C waste-heat and delivering 90 °C hot water.

Importantly, the heat-demand segment plays a relevant role in the CHP exergy efficiency over a long-term operating period (1 year). In fact, even if the ORC-CHP system is designed to maximize the ORC exergy efficiency at a given low-temperature heat demand, the global CHP performance can be significantly decreased when a mismatch between heat sink supply and heat demand mandates that large amounts of cogenerated heat are rendered unusable, which is the case in particular for residential energy demand segments in which CHP systems are optimized for electricity generation, with no thermal storage options. Thus, it is important that the working fluids for these systems are designed with the heat-demand segments and hot-water supply temperatures in mind, with the optimal working-fluids for the design objectives presented in Table 2.

Further research will aim to include energy demand patterns in ORC-CHP working-fluid selection and operational strategy optimization, and to address the trade-offs of costs against performance by means of thermo-economic optimization methodologies, either minimizing the levelized cost of energy and/or maximizing profitability.

Acknowledgements

This work was supported by the UK Engineering and Physical Sciences Research Council (EPSRC) [grant number EP/P004709/1]. O.A. Oyewunmi gratefully acknowledges the PhD funding awarded by the Nigerian government. Data supporting this publication can be obtained on request from cep-lab@imperial.ac.uk.

References

[1] Markides CN. The role of pumped and waste heat technologies in a high-efficiency sustainable energy future for the UK. Appl Therm Eng 2013;53(2):197–209.
[2] Markides CN. Low-concentration solar-power systems based on organic Rankine cycles for distributed-scale applications: overview and further developments. Front Energy Res 2015;3:47.
[3] Oyewunmi OA, Taleb AI, Haslam AJ, Markides CN. On the use of SAFT-VR Mie for assessing large-glide fluorocarbon working-fluid mixtures in organic Rankine cycles. Appl Energy 2016;163:263–82.
[4] Angelino G, Invernizzi C. Cyclic methylsiloxanes as working fluids for space power cycles. J Sol Energy Eng 1993;115(3):130–7.
[5] Chen H, Goswami DY, Stefanakos EK. A review of thermodynamic cycles and working fluids for the conversion of low-grade heat. Renew Sustain Energy Rev 2010;14(9):3059–67.
[6] Drescher U, Brüggemann D. Fluid selection for the organic Rankine cycle (ORC) in biomass power and heat plants. Appl Therm Eng 2007;27(1):223–8.
[7] Oyewunmi OA, Taleb AI, Haslam AJ, Markides CN. An assessment of working-fluid mixtures using SAFT-VR Mie for use in organic Rankine cycle systems for waste-heat recovery. Comput Therm Sci 2014;6(4):301–16.
[8] Lampe M, Kirmse C, Sauer E, Stavrou M, Gross J, Bardow A. Computer-aided molecular design of ORC working fluids using PC-SAFT. Comput Aided Chem Eng 2014;34:357–62.
[9] Lai NA, Wendland M, Fischer J. Working fluids for high-temperature organic Rankine cycles. Energy 2011;36(1):199–211.
[10] Lampe M, Stavrou M, Schilling J, Sauer E, Gross J, Bardow A. Computer-aided molecular design in the continuous-molecular targeting framework using group-contribution PC-SAFT. Comput Chem Eng 2015;81:278–87.
[11] Kirmse CJW, Taleb AI, Oyewunmi OA, Haslam AJ, Markides CN. Performance comparison of a novel thermofluidic organic-fluid heat converter and an organic Rankine cycle heat engine. In Proc: 3rd Int Semin ORC Power Syst 2015.
[12] Kirmse CJW, Oyewunmi OA, Haslam AJ, Markides CN. Comparison of a novel organic-fluid thermofluidic heat converter and an organic rankine cycle heat engine. Energies 2016;9(7):479.
[13] Oyewunmi OA, Markides CN. Thermo-economic and heat transfer optimization of working-fluid mixtures in a low-temperature organic Rankine cycle system. Energies 2016;9(6):448.
[14] Freeman J, Hellgardt K, Markides CN. An assessment of solar-powered organic Rankine cycle systems for combined heating and power in UK domestic applications. Appl Energy 2015;138:605–20.
[15] Freeman J, Hellgardt K, Markides CN. Working fluid selection and electrical performance optimisation of a domestic solar-ORC combined heat and power system for year-round operation in the UK. Appl Energy 2017;186:291–303.
[16] Dong L, Liu H, Riffat S. Development of small-scale and micro-scale biomass-fuelled CHP systems – a literature review. Appl Therm Eng 2009;29(11):2119–26.
[17] Calise F, d'Accadia MD, Vanoli L. Design and dynamic simulation of a novel solar trigeneration system based on hybrid photovoltaic/thermal collectors (PVT). Energy Convers Manage 2012;60:214–25.
[18] Guarracino I, Mellor A, Ekins-Daukes NJ, Markides CN. Dynamic coupled thermal-and-electrical modelling of sheet-and-tube hybrid photovoltaic/thermal (PVT) collectors. Appl Therm Eng 2016;101:778–95.
[19] Ramos A, Chatzopoulou MA, Guarracino I, Freeman J, Markides CN. Hybrid photovoltaic-thermal solar systems for combined heating, cooling and power provision in the urban environment. Energy Convers Manage. http://dx.doi.org/10.1016/j.enconman.2017.03.024.
[20] Tchanche BF, Lambrinos G, Frangoudakis A, Papadakis G. Low-grade heat conversion into power using organic Rankine cycles – a review of various applications. Renew Sustain Energy Rev 2011;15(8):3963–79.
[21] Camporeale S, Ciliberti P, Pantaleo A. Influence of heat demand on techno-economic performance of a natural gas/biomass fired micro gas turbine with bottoming ORC for cogeneration. In: Proc: 3rd Int Semin ORC Power Syst 2015.
[22] Camporeale S, Ciliberti P, Fortunato B, Torresi M, Pantaleo A. Externally fired micro gas turbine and ORC bottoming cycle: Optimal biomass/natural gas CHP configuration for residential energy demand. J Eng Gas Turbines Power 2017;139:1–10. http://dx.doi.org/10.1115/1.4034721.
[23] Pantaleo AM, Camporeale S, Shah N. Natural gas–biomass dual fuelled microturbines: comparison of operating strategies in the Italian residential sector. Appl Therm Eng 2014;71(2):686–96.
[24] Pantaleo AM, Camporeale SM, Shah N. Thermo-economic assessment of externally fired micro-gas turbine fired by natural gas and biomass: applications in Italy. Energy Convers Manage 2013;75:202–13.
[25] Bao J, Zhao L. A review of working fluid and expander selections for organic Rankine cycle. Renew Sustain Energy Rev 2013;24:325–42.
[26] Barse KA, Mann MD. Maximizing ORC performance with optimal match of working fluid with system design. Appl Therm Eng 2016;100:11–9.
[27] Shu G, Li X, Tian H, Liang X, Wei H, Wang X. Alkanes as working fluids for high-temperature exhaust heat recovery of diesel engine using organic Rankine cycle. Appl Energy 2014;119:204–17.
[28] Shu G, Gao Y, Tian H, Wei H, Liang X. Study of mixtures based on hydrocarbons used in ORC (organic Rankine cycle) for engine waste heat recovery. Energy 2014;74:428–38.
[29] Song J, Gu C. Analysis of ORC (organic Rankine cycle) systems with pure hydrocarbons and mixtures of hydrocarbon and retardant for engine waste heat recovery. Appl Therm Eng 2015;89:693–702.
[30] Lampe M, Stavrou M, Bücker HM, Gross J, Bardow A. Simultaneous optimization of working fluid and process for organic Rankine cycles using PC-SAFT. Ind Eng Chem Res 2014;53(21):8821–30.
[31] Imran M, Usman M, Park B-S, Yang Y. Comparative assessment of organic Rankine cycle integration for low temperature geothermal heat source applications. Energy 2016;102:473–90.
[32] Desideri A, Gusev S, van den Broek M, Lemort V, Quoilin S. Experimental comparison of organic fluids for low temperature ORC (organic Rankine cycle) systems for waste heat recovery applications. Energy 2016;97:460–9.
[33] Borsukiewicz-Gozdur A. Experimental investigation of R227ea applied as working fluid in the ORC power plant with hermetic turbogenerator. Appl Therm Eng 2013;56(1–2):126–33.
[34] Kang SH. Design and preliminary tests of ORC (organic Rankine cycle) with two-stage radial turbine. Energy 2016;96:142–54.
[35] Saleh B, Koglbauer G, Wendland M, Fischer J. Working fluids for low-temperature organic Rankine cycles. Energy 2007;32(7):1210–21.
[36] Siddiqi MA, Atakan B. Alkanes as fluids in Rankine cycles in comparison to water, benzene and toluene. In: Proc: 24th Int Conf Effic Cost Optim Simul Environ Impact Energy Syst, ECOS 2011;45(1):256–63.
[37] Schuster A, Karellas S, Kakaras E, Spliethoff H. Energetic and economic investigation of organic Rankine cycle applications. Appl Therm Eng 2009;29(8–9):1809–17.

[38] Tchanche BF, Papadakis G, Lambrinos G, Frangoudakis A. Fluid selection for a low-temperature solar organic Rankine cycle. Appl Therm Eng 2009;29(11–12):2468–76.
[39] Dai Y, Wang J, Gao L. Parametric optimization and comparative study of organic Rankine cycle (ORC) for low grade waste heat recovery. Energy Convers Manage 2009;50(3):576–82.
[40] White MT, Oyewunmi OA, Haslam AJ, Markides CN. Industrial waste-heat recovery through integrated computer-aided working-fluid and ORC system optimisation using SAFT-γ Mie. Energy Convers Manage 2017. http://dx.doi.org/10.1016/j.enconman.2017.03.048.
[41] Calise F, d'Accadia MD, Macaluso A, Piacentino A, Vanoli L. Exergetic and exergoeconomic analysis of a novel hybrid solar–geothermal polygeneration system producing energy and water. Energy Convers Manage 2016;115:200–20.
[42] Bellos E, Tzivanidis C, Antonopoulos KA. Parametric investigation and optimization of an innovative trigeneration system. Energy Convers Manage 2016;127:515–25.
[43] Hosseinpour J, Sadeghi M, Chitsaz A, Ranjbar F, Rosen MA. Exergy assessment and optimization of a cogeneration system based on a solid oxide fuel cell integrated with a Stirling engine. Energy Convers Manage 2017;143:448–58.
[44] Akbari Kordlar M, Mahmoudi SMS. Exergeoconomic analysis and optimization of a novel cogeneration system producing power and refrigeration. Energy Convers Manage 2017;134:208–20.
[45] Zare V. A comparative thermodynamic analysis of two tri-generation systems utilizing low-grade geothermal energy. Energy Convers Manage 2016;118:264–74.
[46] Van Erdeweghe S, Van Bael J, Laenen B, D'haeseleer W. Preheat-parallel' configuration for low-temperature geothermally-fed CHP plants. Energy Convers Manage 2017;142:117–26.
[47] Kolahi M, Yari M, Mahmoudi SMS, Mohammadkhani F. Thermodynamic and economic performance improvement of ORCs through using zeotropic mixtures: case of waste heat recovery in an offshore platform. Case Stud Therm Eng 2016;8:51–70.
[48] Wu Y, Zhu Y, Yu L. Thermal and economic performance analysis of zeotropic mixtures for organic Rankine cycles. Appl Therm Eng 2016;96:57–63.
[49] Vivian J, Manente G, Lazzaretto A. A general framework to select working fluid and configuration of ORCs for low-to-medium temperature heat sources. Appl Energy 2015;156:727–46.
[50] Mavrou P, Papadopoulos AI, Stijepovic MZ, Seferlis P, Linke P, Voutetakis S. Novel and conventional working fluid mixtures for solar Rankine cycles: performance assessment and multi-criteria selection. Appl Therm Eng 2015;75:384–96.
[51] Papadopoulos AI, Stijepovic M, Linke P, Seferlis P, Voutetakis S. Toward optimum working fluid mixtures for organic rankine cycles using molecular design and sensitivity analysis. Ind Eng Chem Res 2013;52(34):12116–33.
[52] Zhao H, Magoulès F. A review on the prediction of building energy consumption. Renew Sustain Energy Rev 2012;16(6):3586–92.
[53] Pedersen L, Stang J, Ulseth R. Load prediction method for heat and electricity demand in buildings for the purpose of planning for mixed energy distribution systems. Energy Build 2008;40(7):1124–34.
[54] Swan LG, Ugursal VI. Modeling of end-use energy consumption in the residential sector: a review of modeling techniques. Renew Sustain Energy Rev 2009;13(8):1819–35.
[55] Giacone E, Mancò S. Energy efficiency measurement in industrial processes. Energy 2012;38(1):331–45.
[56] Bungener S, Hackl R, Van Eetvelde G, Harvey S, Marechal F. Multi-period analysis of heat integration measures in industrial clusters. Energy 2015;93:220–34.